American Mineralogist, Volume 63, pages 1053–1073, 1978

New biopyriboles from Chester, Vermont: II. The crystal chemistry of jimthompsonite, clinojimthompsonite, and chesterite, and the amphibole–mica reaction

DAVID R. VEBLEN[1] AND CHARLES W. BURNHAM

Department of Geological Sciences, Harvard University
Cambridge, Massachusetts 02138

Abstract

The crystal structures of jimthompsonite, clinojimthompsonite, and chesterite have been solved and refined using three-dimensional X-ray intensity data. Jimthompsonite and clinojimthompsonite contain I-beams composed of triple silicate chains and wide octahedral strips. In jimthompsonite these I-beams are stacked like those of orthopyroxenes and orthoamphiboles, while the I-beams of clinojimthompsonite are stacked like those in clinopyroxenes and clinoamphiboles. Chesterite contains both double- and triple-chain I-beams alternating in the *b* direction and assembled in the orthopyroxene–orthoamphibole stacking sequence. The unnamed mineral that occurs as lamellae in chesterite is presumably the monoclinic analog of this structure.

The new minerals are very similar to other low-calcium pyriboles with respect to several crystal-chemical attributes, including polytypism, chain rotation, chain warping, lamellar orientation, and cation ordering patterns. Examination of the outermost polyhedra of chain silicate I-beams suggests that A-chain rotations in orthorhombic pyriboles are a necessary consequence of edge-sharing between tetrahedra and octahedra.

As intermediate reaction products, the new structures delineate a reaction path from anthophyllite and cummingtonite to talc. This amphibole-to-mica mechanism is not simple, but rather proceeds by reconstruction of double-chain I-beams to form alternating double and triple chains, pure triple chains, and finally continuous sheets of silicate tetrahedra.

Introduction

Of the many new minerals described each year, most are not silicates, and those that are usually bear no clear relationship to the important rock-forming mineral groups. The fortuitous discovery of four new minerals that are intimately related to pyroxenes, amphiboles, and micas is thus unusual (Veblen, 1976; Veblen and Burnham, 1975, 1976; Veblen *et al.*, 1977), and the insights into biopyribole crystal chemistry that they provide are profound. A previous paper of this series described the physical and chemical characteristics of the new minerals (Veblen and Burnham, 1978). This paper describes their crystal structures and presents a "comparative anatomy" of the low-calcium biopyriboles.

We begin by describing the development of structural models for the new biopyriboles. The crystal structure refinements of jimthompsonite, clinojimthompsonite, and chesterite will then be presented in turn. Comparisons of biopyribole bond distances and angles, stacking, exsolution directions, chain warping, cation ordering, and chain rotations will follow. Particular attention is given to chain rotations in orthorhombic pyriboles, because this topic has received so much attention in recent years and remains a point of controversy. In the final section of this paper we discuss amphibole–mica reactions in light of the new minerals.

Model derivations

Idealized pyribole I-beams possess either mirror or *c*-glide symmetry. Those containing chains that could be assembled from an even number of pyroxene chains ("even chains") are bisected by mirrors parallel to (010), while those with chains that could be assembled from an odd number of pyroxene chains ("odd chains") are cut by *c*-glides parallel to (010). Both even- and odd-chained ideal I-beams further contain 2-fold axes passing through the M-sites and

[1] Present address: Departments of Geology and Chemistry, Arizona State University, Tempe, Arizona 85281.

0003-004X/78/1112-1053$02.00

Table 1. Crystal data and intensity measurement conditions

	Jimthompsonite	Clino jimthompsonite*	Chesterite
Maximum crystal dimensions, mm.	0.10x0.11x0.52	0.05x0.08x0.40	0.06x0.10x0.35
Crystal volume,** mm^3	0.0044	0.0011	0.0013
Linear absorption coefficient, cm^{-1}	21.0	21.0	20.5
Crystal axis for data collection	c	c	c
2θ scan speed	1°/min.	¼°/min.	1°/min.
Total background counting time	40 sec.	80 sec.	40 sec.

* Clinojimthompsonite crystal data refer to the entire cleavage fragment. Diffraction was from two lamellae (about 10% of the fragment) in jimthompsonite.

** Calculated by absorption correction program, taking account of all planes bounding crystal.

parallel to the *b*-axis, but this rotational symmetry is destroyed if the two chains of an I-beam differ in some way. Ideal odd-chained I-beams (triple, quintuple, *etc.*) are thus symmetrically equivalent to ideal pyroxene I-beams, while even-chained I-beams (quadruple, sextuple, *etc.*) have the same linkage characteristics as amphibole I-beams. These considerations were instrumental in the formulation of structural models for the Chester pyriboles.

The first new mineral to be recognized was chesterite. Like the orthopyroxenes and orthoamphiboles, it was observed to have $a \simeq 18$ and $c \simeq 5\frac{1}{4}$A, and its 45A *b*-axis is an integral multiple of 9A (Veblen and Burnham, 1978, Table 1). The similar intensity distributions on 0-level *b*-axis precession photographs of chesterite, anthophyllite, and enstatite (Fig. 1) indicate that in projection down *b* these structures are closely related. On this basis alone the new mineral was assumed to be a pyribole. Analogous reasoning was used by Warren (1929) and Warren and Modell (1930) to solve the first amphibole structures from their relations to the pyroxenes.

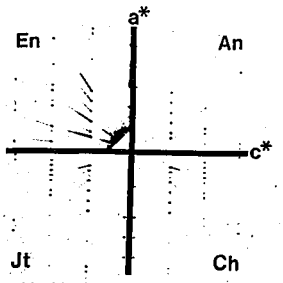

Fig. 1. 0-level *b*-axis precession photographs of enstatite (En), anthophyllite (An), jimthompsonite (Jt), and chesterite (Ch). The similarities in intensity distribution between the four minerals first led to the conclusion that chesterite and jimthompsonite are pyriboles. The vertical direction is a^*, and c^* is horizontal.

Of the space groups consistent with the chesterite diffraction symbol ($A2_1ma$, $Am2a$, $Amma$), only $A2_1ma$ is acceptable as pyribole symmetry; mirrors parallel to (100) are inconsistent with pyribole I-beam topology and linkage operations. The metric requirements and *A*-centering of the cell, and the presence parallel to (010) of both mirrors and *c*-glide planes in the chosen space group, led to the conclusion that the chesterite structure must consist of both even- and odd-chained I-beams, alternating in the *b* direction. There were two possibilities: mixed single and quadruple chains or mixed double and triple chains. The latter was considered more likely.

Soon after the development of the chesterite model, jimthompsonite was discovered. With $b \simeq 27$A (Veblen and Burnham, 1978, Table 1) and space group *Pbca* (the same as orthopyroxene), it was clear that if the reasoning behind the chesterite model was correct, this mineral should consist of triple-chain I-beams arranged in the same fashion as the single-chain I-beams of orthopyroxene. Like chesterite, jimthompsonite closely matched the orthopyribole (*h*0*l*) diffraction intensity distribution (Fig. 1).

Clinojimthompsonite and the unnamed mineral were later discovered as lamellae in jimthompsonite and chesterite. The fact that their *a* dimensions and β angles (Veblen and Burnham, 1978, Table 1) are close to those of low-calcium clinopyroxenes immediately suggested that they are monoclinic polytypes containing triple chains and mixed double and triple chains respectively.

Experimental

The nearly colorless single crystals used for X-ray intensity measurement are elongated in the *c* direction, as a result of their excellent prismatic cleavages. Approximate dimensions of the crystals are listed in Table 1. Because the Chester pyriboles are intergrown with each other, it is not easy to obtain monophase crystals of a size suitable for data collection. The chesterite crystal appeared to be truly monophase, but was small. The jimthompsonite crystal gave extremely weak diffractions from anthophyllite

and chesterite, and precession photographs showed light streaks in the b direction, probably indicating some chain-width disorder. During intensity measurement, these streaks interfered with ($hk0$) reflections with $h/2 + k = 2n + 1$, which were observed to be systematically absent on precession films. These structure factors were therefore removed from the data set, and structure factor calculations using the refined structure later showed that none of these F's have a magnitude above the minimum observable level. The data for clinojimthompsonite were collected from two (100) lamellae in a crystal of jimthompsonite. Each lamella was about 2μ wide, and they were in the same crystallographic orientation. The diffractions from this crystal were sharp, with no evidence of streaking.

Intensity data were measured using a Picker FACS-1 four-circle diffractometer and Nb-filtered Mo$K\alpha$ radiation. They were corrected for Lorentz, polarization, and absorption effects as described by Burnham *et al.* (1971). Scan speeds and background counting times are listed in Table 1. A model-dependent linear absorption coefficient was derived for jimthompsonite, because density and complete chemical data were not available. An electron microprobe analysis and an assumed cell content yielded cation ratios which, when combined with the cell volume, permitted calculation of the linear absorption coefficient. The same value was assumed for clinojimthompsonite, and an absorption coefficient was calculated for chesterite, based again on assumed cell contents. Subsequent refinement of the structures demonstrated the validity of these absorption coefficient calculations. The linear absorption coefficients used for the absorption corrections are listed in Table 1.

Weighting of observations during refinement and minimum observable intensity criteria were the same as those described by Burnham *et al.* (1971), except that the minimum observable intensity for clinojimthompsonite was set at $3\sigma_I$, rather than $2\sigma_I$. Unobserved reflections were excluded from the least-squares normal equations matrices in all cases. Initial scale factors were obtained from a Wilson plot program (Hanscom, 1973).

The three structures were refined with the full-matrix least-squares program RFINE (Finger, 1969), using scattering factors given by Cromer and Mann (1968) for Mg^{2+}, Fe^{2+}, Si^{4+}, and O^{1-}; anomalous dispersion corrections from Cromer and Liberman (1970) were applied to the scattering curves during the final stages of the refinements. The small amounts of Ca^{2+}, Al^{3+}, and Mn^{2+} were ignored in the site occupancy refinements.

Jimthompsonite

Model derivation

Initial atomic coordinates for a trial model of jimthompsonite were derived by cutting the ideal, unrotated orthoenstatite structure along its c-glide planes and inserting additional silicate tetrahedra, octahedral cations, and OH^{1-} ions in a mica-like configuration to form triple-chain I-beams. The I-beam stacking sequence and inter-I-beam linkages of the pyroxene were thus preserved in the model.

Nomenclature for the 29 atoms in the asymmetric unit is shown in Figures 2, 3 and 4. Octahedral cations (M), Si, and O are numbered by starting at the c-glide and counting outward to the edge of the I-beam, in the b direction; the sites analogous to those containing OH^{1-} or F^{1-} in the amphiboles and micas are designated "OH." The Si and O atom labels are

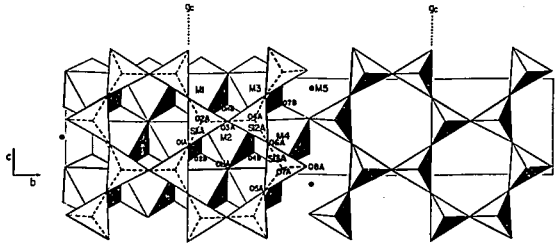

Fig. 2. Triple A-chain of jimthompsonite, projected onto (100). The inner parts of the chain are very straight, while the outer parts are slightly O-rotated. The c-glide is labelled "g_c", and M5 is indicated by solid circles.

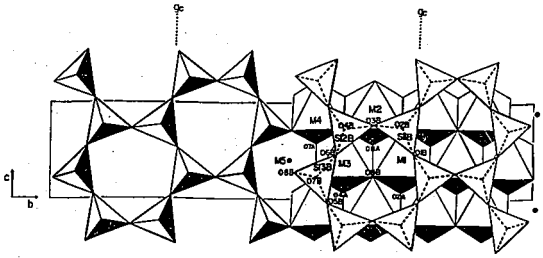

Fig. 3. Projection onto (100) of the *O*-rotated triple B-chain in jimthompsonite. The B-chain clearly is rotated more than the A-chain.

appended by A or B to indicate the tetrahedral chain to which they belong; OH atom labels are similarly appended to indicate on which side of the octahedral bands they are located. As in the orthopyroxenes and orthoamphiboles, the A-chain is cut by a *b*-glide parallel to (100) and lies between octahedral layers of opposite skew, while the B-chain is pierced by 2_1 axes and lies between octahedral layers of like skew (see Thompson, 1970, for definition of skew). The only exception to these rules for atom nomenclature is in the B-chain, where O6B is closer to the *c*-glide than O5B.

Structure refinement

The initial scale factor was refined for one cycle, resulting in R_{weighted} (R_w) = 48.0 percent for the starting model. After five least-squares cycles in which the scale factor and atomic coordinates were allowed to vary, R reached 8.4 percent for 2800 reflections. The scale factor, atom positions, and iso-

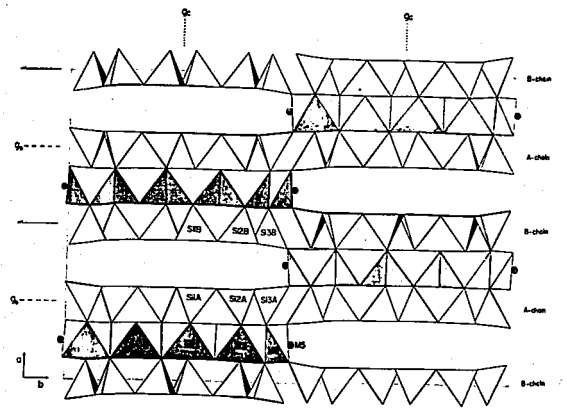

Fig. 4. Jimthompsonite structure projected onto (001). The stacking sequence is ++−−. B-chains occur between octahedral layers of like skew, while A-chains are between layers of opposite skew. The basal oxygen layers of the silicate chains are warped out of the (100) plane. The *c*-glide and *b*-glide are labelled "g_c" and "g_b." M5 is indicated by solid circles, and the unit cell is outlined.

Table 2. Discrepancy factors, *R*, for jimthompsonite, clinojimthompsonite, and chesterite

	Jimthompsonite	Clino-jimthompsonite	Chesterite
All observations:			
Unweighted R[a]	0.121		0.181
Weighted R	0.068		0.066
Number of obs.	6815		6043
Observed diffractions:			
Unweighted R	0.086	0.084	0.091
Weighted R	0.068	0.075	0.059
Number of obs.	4491	769	2633
Unrejected observations:			
Unweighted R	0.084	0.067	0.081
Weighted R	0.057	0.055	0.045
Number of obs.	4457	747	2555
Rejection criterion:	$\Delta F > 20.0$	$\Delta F > 20.0$	$\Delta F > 35.0$

[a] Unweighted $R = \Sigma||F_{obs}|-|F_{cal}||/\Sigma|F_{obs}|$

Weighted $R = [\Sigma\, w(F_{obs}-F_{cal})^2/\Sigma\, wF_{obs}^2]^{\frac{1}{2}}$

tropic temperature factors were then refined for three cycles. Anomalous dispersion corrections were introduced, and the scale factor, atomic coordinates, isotropic temperature factors, and unconstrained M-site occupancies were refined using the complete data set. Final *R* values are given in Table 2. Atomic coordinates, isotropic temperature factors, and M-site occupancies are listed in Table 3, and selected bond distances and angles appear in Table 4a. A more complete listing of distances and angles is in Table 5[2], and observed and calculated structure factors are given in Table 8.

Table 3. Jimthompsonite atom coordinates, temperature factors, and metal (M) site occupancies

Atom	x	y	z	B	Fe/Fe+Mg
M1	0.12565(11)	0.27883(6)	0.89663(35)	0.43(4)	0.060(6)
M2	0.12533(10)	0.33533(6)	0.39366(32)	0.58(4)	0.156(6)
M3	0.12506(12)	0.39257(6)	0.89377(36)	0.42(4)	0.078(6)
M4	0.12485(12)	0.45165(7)	0.39642(37)	0.35(4)	0.011(6)
M5	0.12369(6)	0.50690(4)	0.89507(19)	0.55(2)	0.803(7)
Si1A	0.27111(9)	0.27787(7)	0.55963(27)	0.30(3)	
Si2A	0.26964(10)	0.39005(6)	0.56980(30)	0.49(3)	
Si3A	0.27242(9)	0.44709(6)	0.06669(29)	0.42(3)	
Si1B	0.48025(9)	0.27769(7)	0.26700(28)	0.33(3)	
Si2B	0.48078(10)	0.38929(6)	0.2727B(30)	0.43(3)	
Si3B	0.47579(10)	0.44553(7)	0.77466(30)	0.47(3)	
OHA	0.18329(22)	0.33519(16)	0.06241(69)	0.49(6)	
OHB	0.56861(22)	0.33513(17)	0.76931(69)	0.50(6)	
O1A	0.30061(23)	0.24981(15)	0.31159(73)	0.65(7)	
O2A	0.18399(22)	0.27777(16)	0.56140(69)	0.40(6)	
O3A	0.29949(22)	0.33407(17)	0.55838(70)	0.68(6)	
O4A	0.18325(23)	0.39170(15)	0.56291(74)	0.50(7)	
O5A	0.29980(23)	0.41491(16)	0.82585(78)	0.73(7)	
O6A	0.30187(23)	0.42028(16)	0.33148(77)	0.69(7)	
O7A	0.18560(22)	0.44852(16)	0.06804(74)	0.55(6)	
O8A	0.31330(22)	0.49841(15)	0.08080(77)	0.61(7)	
O1B	0.45141(24)	0.24443(15)	0.03443(70)	0.54(6)	
O2B	0.36718(22)	0.27792(16)	0.26828(69)	0.41(6)	
O3B	0.45168(22)	0.33338(17)	0.23045(70)	0.65(6)	
O4B	0.36725(24)	0.39207(16)	0.27127(75)	0.60(7)	
O5B	0.44881(23)	0.42441(15)	0.05168(74)	0.59(6)	
O6B	0.45138(23)	0.40886(16)	0.54386(77)	0.76(7)	
O7B	0.56296(23)	0.44849(16)	0.77718(74)	0.63(7)	
O8B	0.43394(23)	0.49561(16)	0.71391(75)	0.62(7)	

[2] To obtain a copy of Table 5 (bond distances and angles), order Document AM-78-083, and to obtain Table 8 (structure factors), order Document AM-78-084, from the Business Office, Mineralogical Society of America, 1909 K Street, NW, Washington, DC 20006. Please remit $1.00 in advance for each microfiche.

Table 4a. Selected bond distances and angles in jimthompsonite

M-O Distances, Å

M1 Octahedron		M2 Octahedron		M3 Octahedron	
M1-O2A	2.082	M2-OHB	2.066	M3-OHA	2.097
M1-O2A(1)	2.078	M2-O2A	2.102	M3-OHB	2.078
M1-O2B(2)	2.082	M2-OHA	2.069	M3-O4A	2.070
M1-O2B(3)	2.083	M2-O4A	2.075	M3-O7A	2.104
M1-OHA	2.069	M2-O2B	2.091	M3-O4A	2.066
M1-OHB	2.069	M2-O4B	2.083	M3-O7B	2.120
Mean	2.077	Mean	2.081	Mean	2.089
M4 Octahedron		**M5 Octahedron**			
M4-O4A	2.151	M5-O7A	2.167	M5-O5B	2.938
M4-O4B	2.138	M5-O7B	2.154	Si3A-M5	2.889
M4-O7B	2.080	M5-O8A	2.042		
M4-O7A	2.077	M5-O8B	2.002		
M4-O8A	2.032	M5-O6A	2.443		
M4-O8B	2.048	M5-O6B	2.800		
Mean	2.087	Mean	2.268		

Estimated Standard Error M-O = 0.005Å

Si-O Distances, Å

Si1A Tetrahedron		Si2A Tetrahedron		Si3A Tetrahedron	
Si1A-O1A	1.616	Si2A-O3A	1.624	Si3A-O5A	1.628
Si1A-O1A(1)	1.628	Si2A-O4A	1.610	Si3A-O6A	1.673
Si1A-O2A	1.623	Si2A-O5A	1.617	Si3A-O7A	1.618
Si1A-O3A	1.619	Si2A-O6A	1.622	Si3A-O8A	1.595
Mean	1.621	Mean	1.618	Mean	1.628
Si1B Tetrahedron		**Si2B Tetrahedron**		**Si3B Tetrahedron**	
Si1B-O1B	1.621	Si2B-O3B	1.632	Si3B-O5B	1.654
Si1B-O1B(1)	1.630	Si2B-O4B	1.612	Si3B-O6B	1.643
Si1B-O2B	1.619	Si23-O5B	1.625	Si3B-O7B	1.626
Si1B-O3B	1.619	Si2B-O6B	1.627	Si3B-O8B	1.604
Mean	1.622	Mean	1.624	Mean	1.631

Estimated Standard Error Si-O = 0.005Å

Tetrahedral Chains

A Chain		B Chain	
O1A-O1A-O1A	179.6°	O1B-O1B-O1B	166.9°
O5A-O6A-O5A	173.5°	O5B-O6B-O5B	161.7°

Estimated Standard Error O-O-O = 0.4°

Table 4b. Selected bond distances and angles in clinojimthompsonite

M-O Distances, Å					
M1 Octahedron		M2 Octahedron		M3 Octahedron	
2 M1-OH	2.061	2 M2-OH	2.079	2 M3-OH	2.098
2 M1-O2	2.372	2 M2-O2	2.086	2 M3-O4	2.073
2 M1-O2(4)	2.078	2 M2-O4	2.081	2 M3-O7	2.097
Mean	2.070	Mean	2.082	Mean	2.089
M4 Octahedron		M5 Octahedron			
2 M4-O4	2.128	2 M5-O7	2.162	2 M5-O5	3.106
2 M4-O7	2.081	2 M5-O8	2.032	2 Si3-M5	2.979
2 M4-O8	2.049	2 M5-O6	2.659		
Mean	2.086	Mean	2.284		

Estimated Standard Error M-O = 0.009Å

Si-O Distances, Å					
Si1 Tetrahedron		Si2 Tetrahedron		Si3 Tetrahedron	
Si1-O1	1.628	Si2-O3	1.606	Si3-O5	1.642
Si1-O1(5)	1.627	Si2-O4	1.613	Si3-O6	1.655
Si1-O2	1.634	Si2-O5	1.628	Si3-O7	1.632
Si1-O3	1.616	Si2-O6	1.642	Si3-O8	1.601
Mean	1.626	Mean	1.622	Mean	1.633

Estimated Standard Error Si-O = 0.009Å

Tetrahedral Chain

O1-O1-O1	171.4° ± 0.6°
O5-O6-O5	170.0° ± 0.6°

The jimthompsonite structure

Projections of the refined jimthompsonite structure are shown in Figures 2, 3, and 4. I-beams consisting of triple silicate chains and wide octahedral strips are connected in the orthopyroxene-orthoamphibole + +−− stacking sequence (see Veblen *et al.*, 1977, for an explanation of stacking terminology). Each silicate chain has two symmetrically independent chain rotation angles, an inner rotation angle (O1-O1-O1) and an outer rotation angle (O5-O6-O5), unlike the pyroxenes and amphiboles, which have only one. Both chains are *O*-rotated, the A-chain with inner and outer rotation angles of 179.6° and 173.5°, and the B-chain with inner and outer angles of 166.9° and 161.7°. Chain rotation angles in pyriboles are discussed later in this paper, in light of the new structures; Thompson (1970) explains *O*-rotation *vs. S*-rotations. The silicate chains are topologically distinct from the triple chains in $Ba_2Si_3O_8$, in which alternating apical oxygens point in opposite directions (Katscher and Liebau, 1965; Liebau, 1972).

As in pyroxenes and amphiboles, the outer M-site is a distorted octahedron (M2 in pyroxenes, M4 in amphiboles, and M5 in jimthompsonite), while the inner M-sites are more regular octahedra, slightly compressed in the [100] direction. By further analogy to the low-Ca pyroxenes and amphiboles, Fe^{2+} is concentrated in the outer, distorted M-site, while the regular M-sites favor Mg. The refined Fe/(Fe + Mg) ratio of 0.22 agrees with the (Fe + Mn)/(Fe + Mn + Mg + Ca) value of 0.22 which was measured for this crystal by electron microprobe analysis.

Chain warping or corrugation is apparent in a *c*-axis projection of the structure (Fig. 4). The basal faces of the Si3A and Si3B tetrahedra are tilted significantly out of the (100) plane. The structural significance of pyribole chain warping is discussed in a later section.

Clinojimthompsonite

Model derivations

As shown originally by Warren and Modell (1930), the orthopyroxene unit cell can be closely approximated by two unit cells of clinopyroxene related by a *b*-glide parallel to (100). Since an analogous relationship was hypothesized for jimthompsonite and clinojimthompsonite, the same transformation that Smith (1969) used to relate low clinoenstatite atom coordinates to those of orthoenstatite was used to derive the clinojimthompsonite starting coordinates. The following operation was applied to atoms in one asymmetric unit of the refined jimthompsonite structure:

$$x_{cjt} = 2(x_{jt} - 1/4)$$
$$y_{cjt} = y_{jt}$$
$$z_{cjt} = 1/2 + z_{jt} + (x_{jt} - 1/2)a_{jt}\tan(\beta_{cjt} - 90°)/c_{jt}$$

The resulting $P2_1/c$ model is a triple-chain analog of the low clinoenstatite structure.

Because the observed space group of clinojimthompsonite is $C2/c$, the $P2_1/c$ model was modified by an origin shift and by rotation of the B-chain atoms and OHB ion about the $C2/c$ 2-fold axis. The positions of corresponding atoms in the A- and B-chains were then averaged. The structure described by these average positions, plus the M-sites which lie

Table 4c. Selected bond distances and angles in chesterite

M-O Distances, Å

MT1 Octahedron		MT2 Octahedron		MT3 Octahedron	
MT1-OT2A(6)	2.05	MT2-OHTA	2.10	MT3-OHTA	2.10
MT1-OT2A(7)	2.07	MT2-OHTB	2.06	MT3-OHTB	2.07
MT1-OT2B(8)	2.11	MT2-OT2A	2.11	MT3-OT4A	2.05
MT1-OT2B(9)	2.12	MT2-OT2B	2.10	MT3-OT4B	2.08
MT1-OHTA	2.02	MT2-OT4A	2.09	MT3-OT7A	2.06
MT1-OHTB	2.07	MT2-OT4B	2.04	MT3-OT7B	2.16
Mean	2.07	Mean	2.08	Mean	2.09
MT4 Octahedron		MT5 Octahedron		MD1 Octahedron	
MT4-OT4A	2.16	MT5-OT7A	2.15	MD1-OD1A	2.11
MT4-OT4B	2.16	MT5-OT7B	2.20	MD1-OD1B	2.03
MT4-OT7A	2.07	MT5-OD4A	2.04	MD1-OD2A	2.16
MT4-OT7B	2.10	MT5-OD4B	1.99	MD1-OD2B	2.11
MT4-OD4A	2.00	MT5-OD6A	2.42	MD1-OHDA	2.11
MT4-OD4B	2.02	MT5-OD6B	2.82	MD1-OHDB	2.08
Mean	2.09	Mean	2.27	Mean	2.10
		MT5-OD5B	2.92		
		SiD2A-MT5	2.91		
MD2 Octahedron		MD3 Octahedron		MD4 Octahedron	
MD2-OD1A	2.12	2 MD3-OD1A	2.10	MD4-OD2A	2.19
MD2-OD1B	2.11	2 MD3-OD1B	2.10	MD4-OD2B	2.13
MD2-OD2A	2.10	MD3-OHDA	2.04	MD4-OT8A	2.02
MD2-OD2B	2.06	MD3-OHDB	2.09	MD4-OT8B	2.02
MD2-OT8A	2.07			MD4-OT6A	2.44
MD2-OT8B	2.06	Mean	2.09	MD4-OT6B	2.81
Mean	2.09			Mean	2.27
				MD4-OD5B	2.96
				SiT3A-MD4	2.87

Estimated Standard Error M-O = 0.02Å

Si-O Distances, Å

SiT1A Tetrahedron		SiT2A Tetrahedron		SiT3A Tetrahedron	
SiT1A-OT1A	1.608	SiT2A-OT3A	1.639	SiT3A-OT5A	1.623
SiT1A-OT1A(1)	1.627	SiT2A-OT4A	1.629	SiT3A-OT6A	1.667
SiT1A-OT2A	1.640	SiT2A-OT5A	1.618	SiT3A-OT7A	1.669
SiT1A-OT3A	1.597	SiT2A-OT6A	1.609	SiT3A-OT8A	1.551
Mean	1.618	Mean	1.624	Mean	1.628
SiT1B Tetrahedron		SiT2B Tetrahedron		SiT3B Tetrahedron	
SiT1B-OT1B	1.660	SiT2B-OT3B	1.632	SiT3B-OT5B	1.630
SiT1B-OT1B(1)	1.601	SiT2B-OT4B	1.585	SiT3B-OT6B	1.667
SiT1B-OT2B	1.554	SiT2B-OT5B	1.648	SiT3B-OT7B	1.572
SiT1B-OT3B	1.615	SiT2B-OT6B	1.635	SiT3B-OT8B	1.600
Mean	1.608	Mean	1.625	Mean	1.617
SiD1A Tetrahedron		SiD2A Tetrahedron			
SiD1A-OD1A	1.589	SiD2A-OD2A	1.559		
SiD1A-OD5A	1.599	SiD2A-OD4A	1.647		
SiD1A-OD6A	1.646	SiD2A-OD5A	1.622		
SiD1A-OD7A	1.616	SiD2A-OD6A	1.680		
Mean	1.613	Mean	1.627		
SiD1B Tetrahedron		SiD2B Tetrahedron			
SiD1B-OD1B	1.689	SiD2B-OD2B	1.655		
SiD1B-OD5B	1.604	SiD2B-OD4B	1.618		
SiD1B-OD6B	1.636	SiD2B-OD5B	1.655		
SiD1B-OD7B	1.607	SiD2B-OD6B	1.603		
Mean	1.634	Mean	1.633		

Estimated Standard Error Si-O = 0.018Å

*Coordinate transformations indicated in parentheses:

(1) x, ½−y, ½+z
(2) ½+x, ½−y, 1−z
(3) ½−x, y, 3/2−z
(4) −x, −y, 1−z
(5) x, −y, ½+z
(6) x, y, z−1
(7) x, ½−y, z−½
(8) x−½, ½−y, ½−z
(9) x−½, y, 1−z

Atoms with no transformation indicated are at *xys*, or are participating in an unambiguous distance or angle. Numerals preceeding bonds indicate multiplicity.

Tetrahedral Chains

A Triple Chain		B Triple Chain	
OT1A-OT1A-OT1A	179.6°	OT1B-OT1B-OT1B	167.3°
OT5A-OT6A-OT5A	173.5°	OT5B-OT6B-OT5B	161.1°
A Double Chain		B Double Chain	
OD5A-OD6A-OD5A	170.6°	OD5B-OD6B-OD5B	161.2°

Estimated Standard Error O-O-O = 1.3°

on 2-fold axes, has $C2/c$ symmetry and is a triple-chain analog of high clinoenstatite. It contains 17 atoms in the asymmetric unit and is topologically the same as the NaMg–silicate structure of Drits *et al.* (1974). Site nomenclature in this model is analogous to that for the jimthompsonite structure, except that "A" and "B" are dropped because all triple chains are now symmetrically equivalent.

Structure refinement

Because clinojimthompsonite occurs as lamellae in jimthompsonite, a good single crystal could not be found. Consequently, X-ray intensity data were measured from two (100) lamellae in a jimthompsonite crystal. Because the reciprocal lattice points of the jimthompsonite and clinojimthompsonite overlapped for $l = 4n$, those diffractions were omitted. In spite of long counting times, the measured intensities were very low; thus a large number of diffractions were unobserved. The absorption correction was calculated assuming that the entire crystal was clinojimthompsonite, but because the transmission factors for the entire crystal were high and only varied between 0.88 and 0.93, intensity errors introduced by errors in the absorption correction are small.

In order to check the space-group extinctions, all

Table 6. Clinojimthompsonite atomic coordinates, temperature factors, and metal (M) site occupancies

Atom	x	y	z	B	Fe/Fe+Mg
M1	0.0	0.0289(2)	0.25	0.14(13)	0.033(15)
M2	0.0	0.0869(2)	0.75	0.16(13)	0.041(16)
M3	0.0	0.1428(2)	0.25	0.18(13)	0.095(16)
M4	0.0	0.2013(2)	0.75	0.15(14)	0.008(16)
M5	0.0	0.2569(1)	0.25	0.43(7)	0.845(18)
S11	0.2909(4)	0.0277(2)	0.7656(6)	0.18(5)	
S12	0.2880(4)	0.1395(2)	0.7610(7)	0.24(6)	
S13	0.2971(4)	0.1962(2)	0.2630(7)	0.25(6)	
ON	0.1353(8)	0.0850(3)	0.1566(13)	0.23(12)	
O1	0.3499(11)	0.0037(3)	0.5613(17)	0.42(15)	
O2	0.1356(9)	0.0278(4)	0.6552(15)	0.47(13)	
O3	0.3449(8)	0.0840(3)	0.8197(13)	0.33(11)	
O4	0.1149(10)	0.1420(3)	0.6555(15)	0.48(14)	
O5	0.3535(10)	0.1713(3)	0.0344(15)	0.59(16)	
O6	0.3523(10)	0.1628(3)	0.5390(16)	0.76(15)	
O7	0.1219(9)	0.1983(3)	0.1536(15)	0.45(14)	
O8	0.3777(9)	0.2424(3)	0.3581(3)	0.48(15)	

classes of diffractions were measured. Of 2253 $h + k = 2n + 1$ diffractions, 142 or 6.3 percent were observed (greater than 2σ). If these diffractions were truly extinct, about 5 percent would be expected to be observable at the 2σ level. This is close to what was observed, but refinement was nevertheless first attempted in space group $P2_1/c$, utilizing the $h + k = 2n + 1$ diffractions. Atoms that would have been symmetrically related to each other in $C2/c$ began to move toward $C2/c$-equivalent positions, coordinate correlation coefficients between these atoms became fairly high (about 0.7), and unacceptable bond distances developed. Calculated structure factors for the $h + k = 2n + 1$ diffractions bore no obvious relationship to the low observed structure factors, and R_w did not fall below 10.8 percent. It was concluded that the structure must have $C2/c$ symmetry.

When the criterion for considering a structure factor to be observed was increased to 3σ (of the integrated intensity), only 12 $h + k = 2n + 1$ diffractions remained. These were removed, and the refinement in $C2/c$ converged readily. The scale factor, atomic coordinates, isotropic temperature factors, and unconstrained Mg–Fe occupancies of the M-sites were varied simultaneously during the final cycles of refinement. Only observed diffractions were included in the normal equations. Values of R for clinojimthompsonite are listed in Table 2; atomic positions, isotropic temperature factors, and occupancies are given in Table 6; and selected bond distances and angles are compiled in Table 4b. Tables 5 and 8 (see footnote 2) contain more complete bond distances and angles and the observed and final calculated structure factors for those reflections with $I > 3\sigma_I$.

The clinojimthompsonite structure

Figures 5 and 6 show projections of clinojimthompsonite and present the site nomenclature. The structure consists of I-beams containing five crystallographically distinct M-sites and symmetrically equivalent, *O*-rotated triple silicate chains with inner and outer rotation angles of 171.4° (O1–O1–O1) and 170.0° (O5–O6–O5). These I-beams are connected in a ++++ stacking sequence, analogous to the stacking in monoclinic pyroxenes and amphiboles.

As in the jimthompsonite structure, the inner M-sites are quite regular, but slightly compressed in the [100] direction, while M5, the outer M-site, is a distorted octahedron. Fe is again concentrated over Mg in this distorted outer site; unconstrained occupancy refinement resulted in Fe/(Fe + Mg) = 0.20, while (Fe + Mn)/(Fe + Mn + Mg + Ca + Al_{oct}) = 0.22 was measured with the electron microprobe from the clino lamellae. The I-beams of clinojimthompsonite show the same type of chain warping as those of its orthorhombic polymorph.

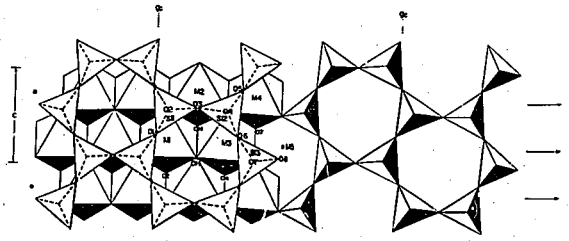

Fig. 5. Projection of clinojimthompsonite onto (100). The triple chain is *O*-rotated.

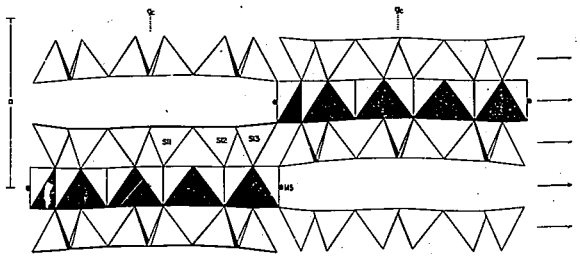

Fig. 6. c-axis projection of the clinojimthompsonite structure. The stacking sequence is ++++, and all triple chains are symmetrically equivalent. As in jimthompsonite, the basal oxygen layers of the silicate chains are warped out of the (100) plane.

Chesterite

Model derivation

An $N(z)$ test using all measured chesterite structure factors resulted in a curve that is acentric at low values of z and hypercentric at z values above 0.3 (Figure 7). Because more than half the data were unobserved and had statistically assigned F^2_{obs} values corresponding to $I_{min}/3$, the intensity averages used in this test are probably incorrect, and the test invalid. In addition, the proposed model for chesterite contained a pseudo-inversion center. The test results were therefore ignored, and a detailed model was constructed in the acentric space group $A2_1ma$, the only space group that is consistent with both the diffraction symbol and pyribole I-beam symmetry and linkage operations.

The chesterite model contains double- and triple-chain I-beams alternating in the b direction and stacked with a ++−− sequence similar to that in other orthopyriboles. Coordinates for an initial structure model were calculated from the refined atom coordinates of jimthompsonite. The triple-chain I-beam of chesterite was taken intact from the jimthompsonite structure, and the double chain was constructed from the Si2, Si3, M2, M3, M4, and M5 polyhedra of the adjacent triple-chain I-beam in jimthompsonite. The following transformation of the appropriate jimthompsonite atoms yielded the model:

$$x_{ch} = x_{jt}$$
$$y_{ch} = 0.6y_{jt} + 0.1$$
$$z_{ch} = z_{jt} + 0.25$$

There are 51 atoms in the asymmetric unit of this structure.

Atom nomenclature in the triple-chain I-beam is the same as that for jimthompsonite, and the nomenclature for the double-chain I-beam follows the standard orthoamphibole terminology (Finger, 1970). Atoms in the tripie-chain I-beams are denoted by "T," and those in the double-chain I-beams by "D." These letters are inserted after the chemical part of the atom names; for example, OT5A is in the A triple chain, while OD5A is in the A double chain.

Structure refinement

After refining only the scale factor for one cycle, R_w for all observed reflections was 0.074, indicating that the model calculated in the above fashion was extremely close to the real structure. After refining scale factor and atom positions for two cycles, convergence was achieved, and R_w reached 0.060 after only minor adjustments in atomic positions.

Isotropic temperature factors and M-site Fe–Mg

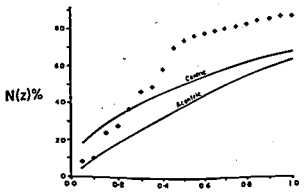

Fig. 7. Plot of the chesterite $N(z)$ test. All measured reflections consistent with diffraction symbol $mmmA--a$ were utilized. See text for interpretation.

occupancies were then refined, and R_w fell to 0.059 for all observed reflections. Atoms in the triple-chain I-beam were, however, strongly correlated with corresponding atoms in the double chains, especially with respect to thermal parameters, which had correlation coefficients as high as 0.8. Analogous atoms within the following polyhedra were strongly correlated: SiD1A and SiT2A; SiD2A and SiT3A; SiD1B and SiT2B; SiD2B and SiT3B; MD3 and MT2; MD1 and MT3; MD2 and MT4; and MD4 and MT5. For example, OD1A, which is the apical oxygen of the SiD1A tetrahedron, was strongly correlated with OT4A, the apical oxygen of the SiT2A tetrahedron. In addition, atoms of the SiT1A and SiT1B tetrahedra exhibited strong correlations with those of all the double-chain tetrahedra, and MT1 was correlated with all other regular M-sites in the structure. Because the above pairs of polyhedra have nearly identical shapes and environments with respect to first- and second-nearest polyhedra, a pseudo-inversion center exists at (1/2, 2/5, 1/4), and there is a pseudo-2_1 axis in the B layers and a pseudo-glide plane in the A layers; this strong pseudo-symmetry is probably responsible for the high correlations. Similar behavior is often noted when refining a structure that deviates only slightly from a higher space-group symmetry [see, for example, Bailey (1975) and Guggenheim and Bailey (1975)]. In chesterite the triple and double chains are topologically distinct, and the pseudo-symmetry is therefore only local.

The isotropic temperature factors of some of the correlated atoms behaved erratically during the refinement, one of a pair assuming a high positive value and the other becoming negative. Because the correlated sites were so similar with respect to both first- and second-nearest neighbors, it was assumed that the atoms occupying them would have similar thermal parameters, and the isotropic temperature factors of corresponding Si, O, and OH ions in the triple and double chains were constrained to be equal. M-site atoms were left unconstrained because of the additional correlations between occupancy and temperature factors. The temperature factors of the constrained atoms attained more reasonable values during this stage of refinement, but M-site temperature factors were still unreasonable. Corresponding M atoms in the D and T I-beams, as listed above, were therefore also constrained to have equal isotropic temperature factors. This resulted in more reasonable thermal parameters and little change in Mg–Fe occupancy; the largest change in an occupancy was 7.6 percent, about $3\sigma_{oc}$. The two unconstrained oxygen atoms in the A triple chain still had negative isotropic temperature factors close to zero. These temperature factors were significantly correlated to the temperature factors of corresponding atoms of all other tetrahedra. It was decided, however, not to pursue any further constraint schemes, because full-matrix least-squares refinement of a 51-atom structure requires large amounts of computer time, and the absolute values of these temperature factors were much less than their standard errors. The changes in atomic positions which resulted from the thermal constraints were insignificant (less than 0.1σ).

Final R values for chesterite are given in Table 2, and atomic coordinates, isotropic temperature factors, and M-site occupancies are listed in Table 7. Because the positional parameters were nearly independent of the thermal and occupancy parameters, the positional standard errors should be realistic. A few of the refined bond distances, such as the SiT3A–OT8A distance of 1.55(2), suggest, however, that these errors are larger. Because the thermal constraints affected occupancies by as much as $3\sigma_{oc}$, the occupancy standard errors are probably several times too low. Likewise, the isotropic temperature factor errors are undoubtedly too low, being based on plausible but unproven constraints that eliminated the largest covariances. The temperature-factor errors were approximately halved by applying the equality constraints.

Because only a small chesterite crystal suitable for intensity measurement could be found, the number of unobserved intensities was large; only 2633 out of the 6043 measured intensities were observed. Structure factor calculations for the unobserved diffractions produced no large F's inconsistent with the structure. The structure refinement of chesterite could undoubtedly be improved if a monophase single crystal large enough to yield a high ratio of observed to unobserved diffractions could be found.

Selected chesterite bond distances and angles are presented in Table 4c. Table 5 contains more complete distances and angles, and the observed and calculated structure factors that were used in the refinement are listed in Table 8 (see footnote 2).

The chesterite structure

Chesterite is the first known chain silicate having more than one set of topologically-distinct chains. The structure is shown in Figures 8, 9, and 10. There are two distinct types of I-beams, one similar to the I-beam of anthophyllite, with A and B double chains, and the other very close to the I-beam of jim-

thompsonite, with A and B triple chains. All the chains are *O*-rotated, except that the inner rotation angle of the A triple chain differs from 180° by less than its standard error. As in jimthompsonite and clinojimthompsonite, the outer tetrahedra of both triple chains are more rotated than the inner ones. The stacking sequence of the I-beams is ++−−, the same as for orthopyroxenes, orthoamphiboles, and jimthompsonite. Because the structure is acentric, there are two nonequivalent ++−− stacking arrangements that are probably equally likely; the atomic positions in Table 7 are for one of these. As in other low-Ca pyriboles, iron is concentrated over magnesium in the distorted outer M-sites, and all four independent chains are warped out of the (100) plane. Occupancy refinement gave overall Fe/(Fe + Mg) = 0.24 for the structure, while electron microprobe analysis gave (Fe + Mn)/(Fe + Mn + Mg + Ca) = 0.26.

Fourier syntheses and A-site occupancies

To confirm the refinement results, electron density difference maps were calculated for all three refined structures. Preliminary difference maps of jimthompsonite and clinojimthompsonite, calculated prior to the application of anomalous dispersion corrections, showed erratic differences as large as 3.5 e/A^3; these differences were eliminated by further refinement using scattering factors corrected for anomalous dispersion, even though R values were not improved.

The final jimthompsonite difference map shows no uninterpretable discrepancies larger than 1 e/A^3. Positive and negative differences indicative of anisotropic thermal motion are associated with M5 (1.8 e/A^3) and with O5A and O6A (1.1 e/A^3). These oxygen difference densities are consistent with tetrahedral torsion about the a^* direction, a type of thermal motion that is observed in other chain silicates. The most pronounced difference peak is located in the position corresponding to the amphibole A-site. This peak is shaped like a lopsided dumbbell with maxima of 3.4 e/A^3 at (0.37, 0.323, 0.89) and 1.3 e/A^3 at (0.37, 0.347, 0.89). The peak, contoured in Figure 11, probably signifies positionally disordered partial occupancy of the A-site. The identity of this site's inhabitants, however, is not so clear; the amount of Na indicated by electron probe analyses of jimthompsonite, including the crystal used for intensity data collection, represents about 2.5 percent Na occupancy, and that amount is not likely to produce a difference density peak as large as the observed one. Small amounts of other species must also be present in the A-site, or the analysis for Na must be too low.

The final difference map for clinojimthompsonite is extremely flat, with no differences greater than ±0.6 e/A^3. The A-site appears to be empty.

The largest differences exhibited by the chesterite difference map are again associated with the A-sites. The AT site, which is sandwiched between the triple-chain I-beams, is slightly split, with two maxima of 1.4 e/A^3 located at (0.36, 0.297, 0.17) and (0.38, 0.307, 0.16). The AD site, on the other hand, has only a single maximum of 1.4 e/A^3 at (0.12, 0.5, 0.61).

Careful examination of the difference maps did not locate H^+ ions in any of the structures.

Table 7. Chesterite atomic coordinates, temperature factors, and metal (M) site occupancies

Atom	x	y	z	B	Fe/Fe+Mg
MT1	0.12670*	0.2675(2)	0.1461(13)	0.38(10)	0.090(15)
MT2	0.1224(7)	0.3013(2)	0.6413(16)	0.82(7)	0.189(15)
MT3	0.1264(6)	0.3357(1)	0.1458(14)	0.30(6)	0.084(13)
MT4	0.1243(6)	0.3715(2)	0.6423(15)	0.33(7)	0.028(13)
MT5	0.1233(5)	0.4044(1)	0.1416(7)	0.41(3)	0.603(13)
SiT1A	0.2704(6)	0.2668(2)	0.8090(11)	0.36(9)	
SiT2A	0.2691(6)	0.3344(2)	0.8169(12)	0.44(5)	
SiT3A	0.2732(6)	0.3682(2)	0.3168(12)	0.43(5)	
SiT1B	0.4811(6)	0.2670(2)	0.5184(12)	0.49(9)	
SiT2B	0.4816(6)	0.3334(2)	0.5245(11)	0.35(5)	
SiT3B	0.4755(6)	0.3678(2)	0.0279(12)	0.43(5)	
CHTA	0.1835(10)	0.3005(4)	0.3086(34)	0.59(14)	
CHTB	0.5695(10)	0.3015(4)	0.0181(34)	0.44(13)	
OT1A	0.2990(8)	0.2499(3)	0.5616(24)	−0.02(17)	
OT2A	0.1823(8)	0.2672(4)	0.8112(26)	−0.06(20)	
OT3A	0.2976(9)	0.3002(4)	0.8001(30)	0.74(13)	
OT4A	0.1817(9)	0.3350(4)	0.8120(28)	0.69(14)	
OT5A	0.2992(9)	0.3690(4)	0.8050(27)	0.92(13)	
OT6A	0.3023(9)	0.3321(4)	0.5806(28)	0.91(13)	
OT7A	0.1836(9)	0.3694(3)	0.3130(30)	0.64(13)	
OT8A	0.3133(8)	0.3982(4)	0.3317(30)	0.37(11)	
OT1B	0.6523(10)	0.2668(4)	0.2777(29)	0.97(25)	
OT2B	0.5665(9)	0.2844(4)	0.5191(26)	0.28(20)	
OT3B	0.4503(9)	0.3091(3)	0.4841(27)	0.39(11)	
OT4B	0.5667(9)	0.3349(4)	0.5234(28)	0.51(13)	
OT5B	0.4497(9)	0.3551(3)	0.3010(26)	0.43(10)	
OT6B	0.4505(9)	0.3454(3)	0.7945(28)	0.69(11)	
OT7B	0.5599(9)	0.3688(3)	0.0326(29)	0.62(13)	
OT8B	0.4365(9)	0.3983(4)	0.9645(30)	0.68(12)	
MD3	0.3718(8)	0.5	0.1485(22)	0.82**	0.214(19)
MD1	0.3771(5)	0.4654(2)	0.6443(16)	0.30	0.057(13)
MD2	0.3749(5)	0.4296(2)	0.1489(18)	0.33	−0.017(13)
MD4	0.3752(5)	0.3963(1)	0.6457(9)	0.41	0.713(13)
SiD1A	0.2302(6)	0.4663(2)	0.3203(13)	0.44	
SiD2A	0.2782(6)	0.4323(2)	0.8125(14)	0.43	
SiD1B	0.5201(6)	0.4664(2)	0.9796(13)	0.35	
SiD2B	0.5246(6)	0.4336(2)	0.4787(14)	0.43	
OHDA	0.3187(13)	0.5	0.8117(66)	0.59	
OHDB	0.4337(13)	0.5	0.6778(67)	0.44	
OD7A	0.2017(13)	0.5	0.3064(64)	0.74	
OD1A	0.3154(10)	0.4647(4)	0.3101(32)	0.69	
OD5A	0.2009(10)	0.4522(4)	0.5770(30)	0.92	
OD6A	0.1974(9)	0.4476(4)	0.0804(30)	0.91	
OD2A	0.3119(9)	0.4316(4)	0.8201(34)	0.64	
OD4A	0.1858(8)	0.4004(4)	0.8281(26)	0.37	
OD7B	0.5442(12)	0.5	0.0268(60)	0.39	
OD1B	0.4294(9)	0.4653(4)	0.9804(31)	0.51	
OD5B	0.5513(9)	0.4457(4)	0.1985(31)	0.43	
OD6B	0.5480(9)	0.4553(4)	0.7028(32)	0.69	
OD2B	0.4357(10)	0.4309(4)	0.4738(33)	0.62	
OD4B	0.5684(9)	0.4035(4)	0.5367(26)	0.68	

* Constrained to fix origin.
** Temperature factors without errors were constrained to equal temperature factors of corresponding atoms in the triple-chain I-beam.

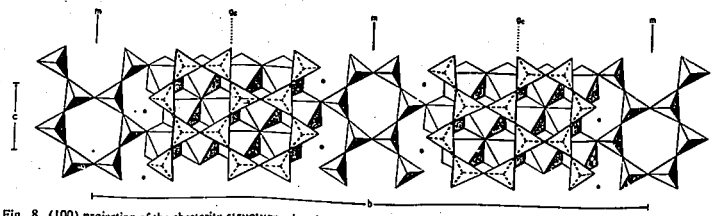

Fig. 8. (100) projection of the chesterite structure, showing the A-chains. Double (D) chains and triple (T) chains alternate in the *b* direction, and all chains are slightly *O*-rotated.

Bond distances and angles

Bond distances and angles in the three refined pyriboles from Chester (Tables 4 and 5) are strikingly similar to the corresponding distances and angles of low-calcium pyroxenes and amphiboles. In this section the tetrahedra and octahedra in the structures of the new minerals are compared with those of anthophyllite (Finger, 1970) and enstatite (Morimoto and Koto, 1969).

The means of all Si-O distances are 1.62A for jimthompsonite, 1.63 for clinojimthompsonite, 1.62 for the triple chains in chesterite, and 1.63 for the chesterite double chains. These values are typical for silicates, and compare with 1.64A for enstatite and 1.63A for anthophyllite. Si-O distances in the new structures appear to be reasonable, except for some of those in chesterite, which are as low as 1.55(2)A and may result from correlation problems in the refinement. The inner tetrahedra (Si1 and Si2) in the triple chains of all three structures are quite regular, as are the T1 tetrahedra in anthophyllite, while the outermost tetrahedra are more distorted, similar to the T2's in anthophyllite and the tetrahedra of orthopyroxenes. In jimthompsonite and clinojimthompsonite, the two shortest Si-O distances of these outer tetrahedra are associated with the longest O-O distance and the widest O-Si-O angle; this is also true of the tetrahedra in many other silicates (Brown and Gibbs, 1970).

The outermost tetrahedron of the A-chain in all orthopyriboles shares an edge with the distorted outer octahedral site. The O-O distance along this shared edge is 2.50A in enstatite and anthophyllite, 2.52 in jimthompsonite, and 2.48 and 2.53 in the chesterite triple chain and double chain, respectively. The analogous edge in clinojimthompsonite is 2.54A. If the outermost M-sites of the octahedral strips are considered to be six-coordinated, then the outermost tetrahedron of the enstatite B-chain shares no edges, while those of the jimthompsonite and chesterite B-chains share one edge. The anthophyllite refined by Finger (1970) is an intermediate case, because the 6th and 7th bonds from M4 to oxygen (O5B and O6B) are the same length within error. This shared tetrahedral edge shortens as it is increasingly shared by the outer M-site: the edge length is 2.59A in enstatite, 2.57 in anthophyllite, 2.55 in jimthompsonite, and 2.56 and 2.53 in the chesterite triple and double chains.

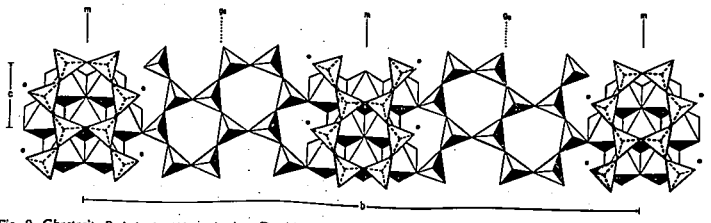

Fig. 9. Chesterite B-chains in (100) projection. Double and triple chains alternate in the *b* direction, and all chains are *O*-rotated.

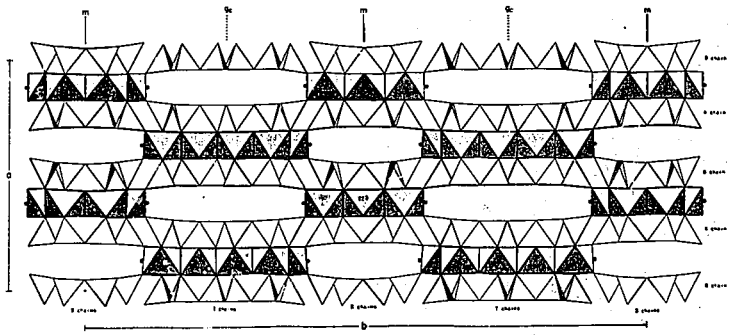

Fig. 10. (001) projection of the chesterite structure. The stacking sequence is ++−−, and I-beams with double and triple chains alternate in the *b* direction. Double and triple B-chains are sandwiched between octahedral layers of like skew, while double and triple A-chains are between layers of opposite skew. Basal oxygen layers of all silicate chains are warped out of the (100) plane.

As in enstatite and anthophyllite, all but the outermost polyhedra of an octahedral strip are quite regular in the refined structures. The most notable departure from regularity is shortening of the edges shared between octahedra. The mean unshared octahedral O–O distances in jimthompsonite and clinojimthompsonite are 3.07A, and the mean for chesterite is 3.08A; the mean shared edge for all three minerals is only 2.81A. By comparison, the unshared edges of the M1 octahedron in enstatite average 3.03A, and the mean of the shared edges is 2.82A. In talc, the means of unshared and shared edges are 3.06A and 2.80A (Rayner and Brown, 1973). The shortening of shared octahedral edges is thus characteristic of low-Ca biopyriboles in all structural groups.

The M–O distances in the outer, distorted octahedra of the three new structures are consistent with occupancy primarily by Fe and Mg. The minimum M–O distances of these sites, and of M2 in enstatite and M4 in anthophyllite, are close to 2.00A (±0.04), much shorter than the analogous distances of calcic pyriboles; the shortest M2–O distance in diopside is 2.35A (Cameron *et al.*, 1973), and the minimum M4–O distance in tremolite is 2.32A (Sueno *et al.*, 1973).

Unnamed mineral

The unit-cell dimensions, space group *A*2/*m* (or *A*2, *Am*), and (*h*0*l*) intensities of the unnamed mineral strongly suggest that it will prove to be the ++++ stacking polymorph of chesterite. If this hypothesis is correct, the structure will have triple-chain I-beams bisected by *c*-glide planes parallel to (010), and double-chain I-beams bisected by mirrors parallel to (010). Such a structure will have space group

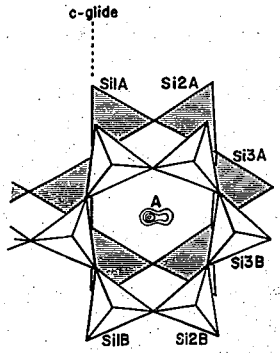

Fig. 11. Difference electron density in the slightly occupied jimthompsonite A-site. The contours, from outer to inner, represent 0, 1, 2, and 3 e/A³. The form of the density differences suggests that there is considerable positional disorder among A-site occupants.

Am if there are two symmetrically distinct silicate chains in each I-beam, and space group *A2/m* if the two chains of each I-beam are related to each other by 2-fold rotation. Since *Am* and *A2/m* exhibit the same diffraction symmetry, either modification of the basic structure may be correct.

The new minerals as biopyriboles

Thompson (1970) explained that most amphiboles can be thought of as 1:1 mixtures of a pyroxene and a mica, sectored along the pyroxene *c*-glides and the mica *a*-glides into (010) slabs, and reassembled. To emphasize the close relationship between these mineral groups, he unearthed Johannsen's (1911) supergroup name, "biopyribole." In addition to 1:1 mixtures (MP), other slab mixtures, such as MMP, might be expected. All mixtures of this sort are biopyriboles, and all belong to a "polysomatic" series of slab mixtures residing in pyroxene–mica compositional space (Thompson, 1978). When viewed in this way, jimthompsonite and clinojimthompsonite are MMP's, and chesterite (and probably the unnamed mineral as well) is an MMPMP.

For an infinite crystal, there are infinite possible polysomes, but the known pyriboles all fall in the following groups: (1) those with pure odd chains of one type (all single chains, or all triple chains, for example); (2) pure even chains (all double, all quadruple chains, *etc.*); or (3) mixed alternating odd and even chains for which the chain numbers differ by 1 (mixed double and triple chains, or mixed single and double chains). Ideal "pure odds" will all have polysome formulas with one P and an even number of M's, and will have space groups *Pbca* or *C2/c*, or their subgroups, for the two common polytypes. "Pure evens" will have formulas with one P and an odd number of M's, and will have maximum symmetries of *Pnma* or *I2/m*. Mixed odd–evens will have two P's and an odd number of M's in the polysome formula, and will have maximum symmetries $A2_1ma$ or *A2/m*. Approximate *b*-axis lengths of these possibilities can be found by multiplying the number of symbols in the polysome formula by 9A. These three possibilities also appear to be the most likely because the mineral reaction sequence at Chester is pure even → mixed even–odd → pure odd; no possibilities such as MMPMMPMP have been observed, and the sequence also suggests that phases such as the MMP's are preferred over MPMMMP's, which would have the same composition.

The existence of chesterite and the unnamed mineral, consisting of mixed double and triple chains, suggests that other mixed-chain silicates intermediate between the pyroxenes and the amphiboles will be found. The most likely phases would be PMP's with space groups $A2_1ma$ or *A2/m* or their subgroups, and having $b \simeq 27$A. The possibility of minerals with chains wider than triple is also intriguing; the fibrous talc of Chester has not yet been examined carefully, and it may be that part of what appears to be talc is really one or more minerals intermediate between jimthompsonite and talc.

It is likely that minerals isostructural with the new biopyriboles from Chester, but having different compositions, will also be found. This possibility is enhanced by the synthesis of a *C2/c*, NaMg triple-chain silicate by Drits *et al.* (1974, 1976). This fibrous phase is reported to contain Na in the M5 site and OH^{1-} replacing tetrahedral O^{2-}; it is therefore not a true biopyribole, but would be similar to "hydroamphiboles" and could be thought of as a slab mixture of talc and NaMg "hydropyroxene." Similar phases that are true biopyriboles could exhibit the wide range of ionic substitutions observed in the pyroxenes, amphiboles, and micas, as could minerals isostructural with chesterite. The new minerals from Chester may simply be low-calcium members of two large, but heretofore unrecognized, mineral groups. It is expected that the orthorhombic structure types will be restricted to compositions containing only small amounts of Ca or other large octahedral cations.

Polytypism

Pyribole polytypism has long been a subject of interest to mineralogists and petrologists. The compositional and intensive-parameter stability ranges of the enstatite polymorphs, and of anthophyllite and cummingtonite, are still not agreed upon. Although they in no way solve the stability problem, the new pyriboles from Chester are of interest in that they possess the two most common stacking sequences of the pyroxenes and amphiboles: chesterite and jimthompsonite are stacked in the same manner as the orthopyroxenes and orthoamphiboles, while clinojimthompsonite and probably the unnamed phase have stacking sequences analogous to those of the clinopyroxenes and clinoamphiboles.

The new orthorhombic pyriboles have ++−− stacking, while the new clinopyriboles are stacked ++++ (see Veblen *et al.*, 1977, for an explanation of this stacking terminology). No pyriboles from Chester were found to have a proto stacking sequence (+−+−). In addition, none of the 88 single crystals

examined by precession photography showed evidence of streaking in the direction of a^*, which would signify fine-scale stacking disorder.

Pyribole chain rotations and the parity rule

Tetrahedral rotations play an important role in sheet silicates (Bailey, 1966; Bailey *et al.*, 1967). In micas, the primary influence on the degree of rotation is apparently the requirement that the tetrahedral and octahedral layers occupy the same area (McCauley and Newnham, 1971). In addition to these dimensional requirements, the tetrahedral rotations of chain silicates are further subject to restrictions arising from connections between I-beams. One formulation of these additional requirements is the parity rule (Thompson, 1970; Papike and Ross, 1970), which states that in ideal pyriboles having regular polyhedra except for the outer M-site, geometrical constraints are imposed on tetrahedral rotations by the octahedral stacking sequence. Chains between octahedral layers of like skew (here defined as ·-chains) must be straight, or have the same rotation sense, while chains between layers of opposite skew (defined as x-chains) must be straight, or have *O*- and *S*-rotations alternating in the *b* direction. This rule is rigorous for regular polyhedra and must be strictly obeyed, even for small tetrahedral rotations. The polyhedra of real pyriboles are not perfectly regular, however, and in this section we will show that violations of the parity rule are a necessary consequence of distortions arising from edge-sharing among polyhedra.

Rotations and symmetry of real orthopyriboles

It has been pointed out that the A-chains of refined orthopyriboles and the chains of protopyriboles, which are located between octahedral layers of opposite skew, are all *O*-rotated, and that they therefore violate the parity rule. Papike and Ross (1970) explained that the parity violations of gedrites are accompanied by M2 distortion, and that the A-chains are less rotated than the B-chains. Papike *et al.* (1973) discussed parity violations in orthopyroxenes and concluded that the violations are minimized by extentional rotation (straightening) of the chains. They also suggested that the outer-M-site (M2) coordination requirements necessitate the A-chain *O*-rotations. Sueno *et al.* (1976) further explain that polyhedral distortions permit parity violations.

It has been suggested that parity violations do not, in fact, occur and that the space groups of real orthopyroxenes and orthoamphiboles may be $P2_1ca$ and $P2_1ma$, rather than *Pbca* and *Pnma*, thus allowing the A-chains to have alternating *O*- and *S*-rotations (Thompson, 1970). These alternative space groups would, however, be readily differentiated with single-crystal X-ray methods. An orthopyroxene with $P2_1ca$ symmetry has been reported (Smyth, 1974), but the intensities of equivalent violating reflections (the {071} diffractions, for example) are not equal in the published precession photograph and do not even possess inversion symmetry. Furthermore, orthopyribole refinements of average structures should exhibit strongly anisotropic thermal motion, which is not observed. Chesterite has been refined in a space group that does not require the parity-violating A-chains to have the same sense or degree of rotation in adjacent chains, yet the parity rule is still violated with *O*-rotated A-chains having chain angles of 173.5° and 170.6°. We therefore conclude that orthopyroxene and jimthompsonite refinements in *Pbca*, and orthoamphibole refinements in *Pnma*, are correct.

The cause of orthopyribole A-chain rotations

The triple chains of the new minerals from Chester provide new information on the causes of pyribole chain rotations. In all cases the interior and more mica-like part of the chain is less rotated than the outer part, suggesting that the rotations, at least of the outer tetrahedra, result primarily from the requirements of inter-I-beam connection geometry. The same effect is observable in the amphiboles, though not so graphically as in the pyriboles with triple chains. In the following discussion we therefore concentrate on the outermost polyhedra along the edges of pyribole I-beams.

If the chains between octahedral layers of opposite skew (x-chains) are all equivalent, as they are in real pyriboles, and if the inner M polyhedra are perfectly regular, then the two non-bridging oxygens of the outermost tetrahedron of the chain must project orthogonally onto the same point of any line that describes the chain direction (the *c*-axis, for example). The appropriate atoms are O1A and O2A for the pyroxenes, O2A and O4A for the amphiboles, and O7A and O8A for pyriboles with triple chains. In the orthorhombic pyriboles, this requirement simply means that these atom pairs must have the same z coordinate. In a real orthorhombic pyribole, the amount of "misfit" exhibited by the outer x-chain tetrahedron can be defined as the difference, in Å, between the z coordinates of these two atoms. This misfit must be absorbed by distortion of the regular inner M octahedra.

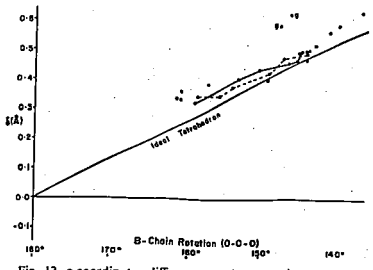

Fig. 12. z-coordinate difference (δ) between the two non-bridging oxygens of the outermost A-chain tetrahedron in refined proto- and orthopyriboles, plotted against the A-chain rotation angle. The difference, δ, is a "misfit" parameter for the A-chains and must be absorbed by distortion of the regular octahedra. The line marked "Ideal Tetrahedron" shows the amount of misfit that would be produced by rotation of a chain of regular tetrahedra; most orthopyriboles have misfits with opposite sign from that predicted. The points marked "g" refer to gedrite structures (Papike and Ross, 1970), and the points connected by continuous and broken line segments refer to orthopyroxene structures at several temperatures (Smyth, 1973; Sueno *et al.*, 1976; respectively), the chain becoming straighter with increasing temperature. Other data are from Burnham (1967), Burnham *et al.* (1971), Finger (1970), Ghose (1965), Gibbs (1969), Kosoi *et al.* (1974), Morimoto and Koto (1969), Morimoto *et al.* (1975), Smyth (1971), Smyth and Ito (1977), Takeda (1972), and this paper.

The amount of misfit produced by a regular tetrahedron is

$$\delta = 2\sqrt{2}/3\ (\text{T–O})\sin\tfrac{1}{2}(180° - \text{RA})$$

where (T–O) is the tetrahedral cation–oxygen distance, and RA is the rotation angle as traditionally measured for chain silicates (*e.g.* O3–O3–O3 for pyroxenes). The expected misfit for T–O = 1.62A is plotted as a function of rotation angle in Figure 12, along with the real misfit exhibited by the x-chains of orthorhombic pyriboles with dominantly divalent cations in the outer M-sites. No attempt was made to include standard errors in the diagram, but the errors are small enough in all cases so that the conclusions are not altered.

Figure 12 shows that the tetrahedral misfit in real pyriboles generally has the opposite sign and is much smaller than that predicted for chains of regular tetrahedra. This means that the misfit would be *increased* by extending the chains, and *decreased* by rotating them further. Consequently greater, not less, *O*-rotation would permit the inner M-sites to be perfectly regular. The only exceptions to this pattern are the gedrites.

Figure 13 compares the A-chain of XYZ orthopyroxene (Burnham *et al.*, 1971) with a chain of ideal tetrahedra having the same rotation angle. It is clear that distortion of the pyribole outer tetrahedra accounts for the nonideal magnitude and sign of the A-chain misfit, and it is apparent that this distortion arises to a large degree from edge-sharing with the outer M-site. The O–O distance for this shared edge is close to 2.50A in all refined orthopyriboles; this is a typical value for shared polyhedral edges in many types of compounds (Pauling, 1948, p. 400). It is certainly not surprising that the outer tetrahedra of orthopyribole A-chains are distorted by edge-sharing, and if distortions of the inner M octahedra are to be minimized, then it is essential that the A-chains be *O*-rotated. This is indeed the case.

The only refined pyribole structures with tetrahedral misfit having the same direction as that predicted by an ideal polyhedral model are those of gedrite (Papike and Ross, 1970). These are the only phases

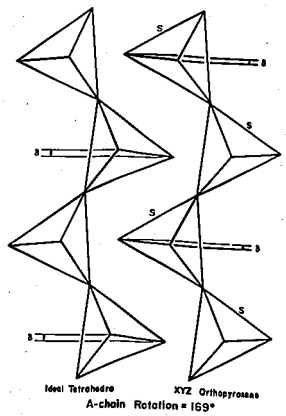

Fig. 13. A real orthopyroxene A-chain with rotation angle O3–O3–O3 of 169° (Burnham *et al.*, 1971), compared with a chain of ideal tetrahedra having the same sense and degree of rotation. The short shared edges of the real tetrahedra are marked "S." The figure shows how tetrahedral distortion accounts for the small misfit (δ) in the real A-chain, so that straightening of the chain would necessitate increased, rather than decreased, distortion of the regular M octahedra.

plotted in Figure 12 with significant A-site occupancy, and the difference in the tetrahedral misfit of the gedrite A-chains is consistent with the ditrigonal distortion that is expected to arise from A-site bonding requirements.

B-chain rotations in orthopyriboles

The parity rule states that for tetrahedral chains between octahedral layers of like skew (--chains), all chains in a layer must have the same sense and degree of rotation. In all known orthopyriboles except chesterite all of the --chains (B-chains) are symmetrically equivalent, and, except for this equivalence and the requirement that the chains and octahedral strips of an I-beam must fit together, there are no rigid geometrical constraints on rotations. Inter-I-beam misfit constraints do not apply to orthopyribole B-chains; hence they can assume larger rotation angles than are permitted in the A-chains.

Figure 14 shows that differences in outer nonbridging oxygen z coordinates in orthopyribole B-chains are much better predicted by chain rotation angle than they are for the A-chains, as a result of the greater regularity of the B-chain outer tetrahedra. There appears to be a tendency for the difference to be slightly larger than predicted, resulting partly from shortening of a tetrahedral edge. It should be noted that this edge is shared with the outer M-site in some orthopyriboles, but not in others, as discussed in the next section. The edge shortening suggests that there is some degree of bonding between the outer M-site and the distant bridging oxygen of the outer tetrahedron, even when this oxygen is not one of the metal ion's six or seven nearest neighbors.

Conclusions on pyribole chain rotations

Because the real misfit in pyribole x-chains is small, and since the rotation of these chains reduces the misfit, it can be concluded that these rotations arise largely as a result of tetrahedral edge-sharing distortions. The smaller rotations of the inner tetrahedra of triple chains suggest that intra-I-beam effects tend to straighten the chains, preventing them from achieving a zero-misfit configuration. If it is recognized that this misfit is generally small in the pyriboles, then it must also be realized that parity violations pose no problem for the real structures. Because there are no major misfit difficulties, there is no compelling reason to expect the existence of ortho- and protopyriboles with alternating *O*-rotated and *S*-rotated x-chains.

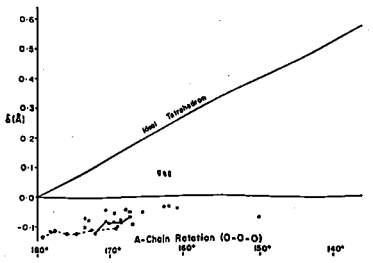

Fig. 14. z-coordinate difference (δ) between the two nonbridging oxygens of the outermost B-chain tetrahedron in refined orthopyriboles, plotted against the B-chain rotation. Most of the structures have δ slightly larger than an ideal tetrahedron with the same rotation angle, owing to tetrahedral distortion. The two points marked "g" are gedrites, and points connected by continuous and broken line segments refer to orthopyroxene structures at several temperatures (Smyth, 1973; Sueno *et al.*, 1976), the chain becoming straighter with increasing temperature. Other data are from the same references as those of Fig. 12.

Outer M-site coordination

If the outer M-sites of pyriboles are considered to be six-coordinated, there are two distinct coordination types for these sites. This is perhaps best demonstrated by a series of high-temperature orthopyroxene refinements by Smyth (1973), who showed that there is an M2 coordination switch from O3B to O3B′ between 700° and 850°C. This behavior was confirmed in orthoferrosilite by Sueno *et al.* (1976). The higher-temperature coordination involves the sharing of not only an A-chain tetrahedral edge, but also a B-chain edge, and is a configuration similar to that in protopyroxenes and $C2/c$ clinopyroxenes. The coordination change is analogous to the one observed to take place during the $P2_1/c$–$C2/c$ clinopyroxene transformation (Smyth and Burnham, 1972; Brown *et al.*, 1972).

The gedrite structures refined by Papike and Ross (1970) have outer M-site coordinations that are close to those of low-temperature orthopyroxenes. In contrast, the anthophyllite structure refined by Finger (1970) exhibits an intermediate configuration in that O5B and O6B are equidistant from M4.

The outer M-sites of jimthompsonite (M5) and chesterite (MT5 and MD4) possess the high-temperature orthopyroxene M2 configuration. They share tetrahedral edges with both the A- and B-chains. On purely geometrical grounds it is obvious that those

orthopyriboles with straighter B-chains will tend to the higher-temperature configuration, while those that have more kinked chains will tend to the lower-temperature outer M-site coordination. All orthopyriboles refined at room temperature with B-chains straighter than those of Finger's (1970) anthophyllite (O5B–O6B–O5B = 157.5°) do have the higher-temperature outer-site coordinations, while all those with more rotated B-chains resemble room-temperature orthopyroxene. In orthoferrosilite the coordination switch occurs when O3B–O3B–O3B ≃ 151° (Sueno *et al.*, 1976). There also seems to be a tendency for orthopyriboles with wider chains to have smaller rotation angles, and therefore the higher temperature outer M-site coordination.

Polytype stabilities

Much has been made of the importance of outer M-site coordination to pyribole stability ranges. Papike *et al.* (1973) suggest that pyroxene M2 coordination controls the ortho–clino transformation, and that $P2_1/c$ pyroxenes form metastably because their M2 sites have the low-temperature ortho coordination. Smyth (1973) concurs with this notion, and further suggests that the inability of the *Pbca* orthopyroxene structure to attain a higher symmetry configuration reduces its stability at high temperatures relative to the monoclinic structure, which transforms from $P2_1/c$ to the higher $C2/c$ symmetry.[3] The outer-site coordination must exercise some control over the stabilities of the various polytypes, because pyriboles with large cations occupying these sites never occur in the orthorhombic forms. However, it seems unlikely that the relative positions of the outer M cations and their most distant coordinating oxygens can completely control the thermodynamic behavior of the magnesian pyriboles. Other factors may also affect the relative stabilities.

The data of Sueno *et al.* (1976) and Smyth (1973), which are shown on Figure 12, suggest that A-chain misfit in orthopyroxene increases with rising temperature. It is possible that the regular octahedra of the structure are unable to deform enough to absorb this misfit, and that this inability is in part responsible for reconstruction to the $C2/c$ structure, which has no x-chains and therefore no chain misfit constraints.

[3] Monoclinic $C2/c$ pyroxenes must be considered to possess higher symmetry than orthorhombic *Pbca* ones, because the density of symmetry elements is greater, and hence there are fewer atoms per asymmetric unit. Also the M-site coordination polyhedra possess higher point symmetry.

Chain warping

Basal oxygen layers of all the chains in the Chester biopyriboles are "warped" out of the (100) plane, as can be seen in Figures 4, 6, and 10. The same phenomenon also occurs in pyroxenes and amphiboles.

A measure of the degree of warping in orthopyriboles is the maximum difference, in A, between the x coordinate of the outmost oxygen of the chain and the x coordinate of the other basal oxygens. The amounts of warping in enstatite (Morimoto and Koto, 1969), anthophyllite (Finger, 1970), jimthompsonite, and chesterite are shown in Table 9. The chains of enstatite are not so warped as those of the wider chain silicates, and the double B-chains of anthophyllite and chesterite are more warped than any of the single or triple B-chains.

The distances between basal oxygen layers in the double- and triple-chain pyriboles are roughly equivalent to the inter-layer basal oxygen distances of talc (Rayner and Brown, 1973), except for near the chain edges, where bonding within the adjacent M octahedra pulls the chains together. If the warping were the result of octahedral–tetrahedral misfit, as in the antigorites, one would expect the triple-chain basal oxygen layers of jimthompsonite, clinojimthompsonite, and chesterite to be uniformly bent. Instead, most of the warping occurs in the outermost tetrahedron, and the interior mica-like parts of the basal layer are quite flat.

Lamellae orientation

All specimens of clinojimthompsonite and the unnamed mineral that have been observed from the Chester wall zone occur as (100) lamellae in jimthompsonite and chesterite, respectively. This is the same orientation that is commonly seen in intergrowths of orthorhombic and monoclinic pyroxenes and amphiboles. The (100) ortho–clino orientation is probably common to all the known pyribole groups because nearest-neighbor coordinations at the boundary between two polytypes sharing (100) are nearly the same as in the two structures away from the boundary; only second-nearest-neighbor relationships are upset.

Cation ordering

Refinement of M-site Mg–Fe occupancies for jimthompsonite, clinojimthompsonite, and chesterite reveals the same ordering pattern observed in the low-calcium pyroxenes and amphiboles: Fe^{2+} is concentrated in the outer, distorted sites, while Mg prefers the inner, more regular sites. This is an expected

result, as the outer M-site polyhedral geometries and environments are similar for all the ferromagnesian pyriboles, when only the five oxygens nearest this site are considered; the differences in the sixth- and seventh-nearest oxygens, as previously discussed, appear to have little consequence for Mg–Fe ordering tendencies. The M4 site of triple-chain I-beams, which is analogous to the M2 site of amphiboles, appears to be slightly enriched in Mg compared with the other regular octahedral sites.

The amphibole–mica transformation

Many pyribole single crystals from Chester produce streaks parallel to b^* on precession films, indicating some degree of structural disorder in the b direction. Preliminary results from high-resolution electron microscopy have shown that the streaking results from errors in the widths of silicate chains in the ordered minerals and from regions with apparently random sequences of double, triple, and wider chains (Veblen *et al.*, 1977). Work is now in progress to fully characterize the microstructures found in pyriboles from Chester.

The X-ray results on the new minerals show us the general pattern of the amphibole–mica reaction. Rather than being a simple one-step reaction, the anthophyllite–talc transformation is, at least in the Chester wall zone, a complex multistage reaction. The following sequence can be inferred from the petrographic, chemical, and diffraction data on the Chester biopyriboles.

1. Anthophyllite becomes structurally disordered, acquiring triple-chain structure at random intervals; Fe^{2+} and Mg^{2+} diffuse out of the structure as H^+ diffuses in.
2. When a region of the structure has a high enough concentration of triple chains, it begins to order into chesterite or its monoclinic analog. Because these structures contain rigorously alternating double- and triple-chain slabs, the transformation from a disordered chain sequence to these minerals must entail considerable reconstruction.
3. More triple chains form, in excess of the 1:1 double:triple ratio found in chesterite. More structurally disordered states are the result.
4. When all the double chains have been consumed, the transformation to the ordered triple-chain minerals jimthompsonite and clinojimthompsonite is complete.
5. Talc grows at the expense of jimthompsonite. It is not yet known whether this growth mechanism is simple or whether it entails formation of still more ordered intermediate structures.

Table 9. Degree of chain warping (A) in low-Ca orthopyriboles

	A chain	B chain	Mean
Enstatite	0.14(2)	0.24(2)	0.19
Anthophyllite	0.29(2)	0.41(2)	0.35
Jimthompsonite	0.26(2)	0.28(2)	0.27
Chesterite: T-chains	0.29(3)	0.33(4)	0.31
D-chains	0.29(4)	0.45(4)	0.37

Several implications of the above reaction scheme deserve comment. Because the transformation from pure double chains to pure triple chains proceeds through an ordered mixed-chain intermediate, it is possible that pyroxene–amphibole reactions produce alternating single-double chain phases. In addition, these reactions are likely to be marked by structurally disordered states.

It has not, of course, been determined whether these minerals have stability fields of their own. Because they occur in considerable quantities (the new orthorhombic phases can exceed 1mm in a and c dimensions and reach several hundred microns in the b direction), they must be "nearly stable," even if they formed metastably. The question of stability is moot in any case, because the biopyriboles of the Chester wall zone include at least seven intimately coexisting phases which are apparently chemically co-linear and may include three compositional coincidences: this is not an equilibrium state of affairs. The new pyriboles will probably never attain valuable petrogenetic indicator status.

It is not clear whether the reverse reaction, from talc to anthophyllite, takes place by the reverse mechanism, but there is some evidence that the path may be similar. Daw *et al.* (1972) found in a TEM study that enstatite formed by heating talc produced electron diffraction patterns that were heavily streaked in the b direction. They also observed (010) planar "faults" in the enstatite, reminiscent of the (010) lamellar features observed in the Chester pyriboles. Greenwood's (1963) rate study on growth of enstatite from talc further indicates that anthophyllite is an intermediate product, and other phases could have been lurking in the run products disguised as anthophyllite or enstatite. In any case, mica to pyroxene reactions appear to take place by a complex mechanism, rather than a single step.

The inferred anthophyllite–talc reaction sequence points out major problems in biopyribole reactions. The intergroup reactions are controlled by multistep,

highly reconstructive mechanisms, at least at metamorphic temperatures and time scales. Kinetic difficulties have already been recognized in experimental studies: Greenwood (1963) was unable to nucleate anthophyllite from talc in the anthophyllite stability field, but anthophyllite nucleated easily in parts of the enstatite stability range.

Conclusion

It is hoped that this paper will encourage petrologists and mineralogists who deal with biopyriboles to be cautious in their observations. Chain-width faulting may prove to be commonplace in all the biopyribole groups, altering thermochemical as well as physical properties. Structurally-ordered minerals intermediate between the pyroxenes, amphiboles, and micas may prove to be common minor phases, but their identification requires a combination of careful petrographic, X-ray, and chemical observations on fine-grained material. This would perhaps come as no surprise to Johannsen (1911), who, in giving the supergroup the name "biopyribole," recognized that they all look very much alike.

Acknowledgments

This paper bears the clear mark of James B. Thompson's theoretical work on biopyriboles. We thank him warmly for our discussions and for his shared insights. We also thank James F. Hays, John B. Brady, Richard Sanford, and Kenneth Shay for useful conversations. This work represents part of a Harvard University Ph.D. thesis (Veblen, 1976). The final version of the paper was improved by thorough reviews from James J. Papike and Cornelis Klein. Financial support for this research was provided by NSF grant GA-41415 to Charles W. Burnham.

References

Bailey, S. W. (1966) The status of clay mineral structures. *Proc. Nat. Conf. Clays and Clay Minerals, 14,* 1–23.

—— (1975) Cation ordering and pseudosymmetry in layer silicates. *Am. Mineral., 60,* 175–187.

——, G. W. Brindley, W. D. Keller, D. R. Wones and J. V. Smith (1967) *AGI Short Course Lecture Notes—Layer Silicates.* American Geological Institute, Washington.

Brown, G. E. and G. V. Gibbs (1970) Stereochemistry and ordering in the tetrahedral portion of silicates. *Am. Mineral., 55,* 1587–1607.

——, C. T. Prewitt, J. J. Papike and S. Sueno (1972) A comparison of the structures of low and high pigeonite. *J. Geophys. Res., 77,* 5778–5789.

Burnham, C. W. (1967) Ferrosilite. *Carnegie Inst. Wash. Year Book, 65,* 285–290.

——, Y. Ohashi, S. S. Hafner and D. Virgo (1971) Cation distribution and atomic thermal vibrations in an iron-rich orthopyroxene. *Am. Mineral., 56,* 850–876.

Cameron, M., S. Sueno, C. T. Prewitt and J. J. Papike (1973) High-temperature crystal chemistry of acmite, diopside, hedenbergite, jadeite, spodumene, and ureyite. *Am. Mineral., 58,* 594–618.

Cromer, D. T. and D. Liberman (1970) Relativistic calculation of anomalous scattering factors for X-rays. *J. Chem. Phys., 53,* 1891–1898.

—— and J. B. Mann (1968) X-ray scattering factors computed from numerical Hartree-Fock wave functions. *Acta Crystallogr., A24,* 321–324.

Daw, J. D., P. S. Nicholson and J. D. Embury (1972) Inhomogenous dehydroxylation of talc. *J. Am. Ceram. Soc., 55,* 140–151.

Drits, V. A., Yu. I. Goncharov, V. A. Aleksandrova, V. E. Khadzhi and A. L. Dmitrik (1974) New type of strip silicate. *Kristallografiya, 19,* 1186–1193. (transl. *Sov. Phys. Crystallogr., 19,* 737–741).

——, —— and I. P. Khadzhi (1976) Formation conditions and physico-chemical constitution of triple chain silicate with $[Si_6O_{18}]$ radical. (in Russian) *Izvestiya Akad. Nauk., Ser. Geol., No. 7,* 32–41.

Finger, L. W. (1969) Determination of cation distribution by least-squares refinement of single-crystal X-ray data. *Carnegie Inst. Wash. Year Book, 67,* 216–217.

—— (1970) Refinement of the crystal structure of an anthophyllite. *Carnegie Inst. Wash. Year Book, 68,* 283–288.

Ghose, S. (1965) Mg^{2+}–Fe^{2+} order in an orthopyroxene, $Mg_{0.91}Fe_{1.09}Si_2O_6$. *Z. Kristallogr., 122,* 81–99.

Gibbs, G. V. (1969) Crystal structure of protoamphibole. *Mineral. Soc. Am. Spec. Pap., 2,* 101–109.

Greenwood, H. J. (1963) The synthesis and stability of anthophyllite. *J. Petrol., 4,* 317–351.

Guggenheim, S. and S. W. Bailey (1975) Refinement of the margarite structure in subgroup symmetry. *Am. Mineral., 60,* 1023–1029.

Hanscom, R. H. (1973) *The Crystal Chemistry and Polymorphism of Chloritoid.* Ph.D. Thesis, Harvard University, Cambridge, Massachusetts.

Johannsen, A. (1911) Petrographic terms for field use. *J. Geol., 19,* 317–322.

Katscher, H. and F. Liebau (1965) Uber die Kristallstruktur von $Ba_6Si_6O_{18}$, ein Silikat mit Dreifachketten. *Naturwissenschaften, 18,* 512–513.

Kosoi, A. L., L. A. Malkova and V. A. Frank-Kamenetskii (1974) Crystal-chemical characteristics of rhombic pyroxenes. *Kristallografiya, 19,* 282–288. (transl. *Sov. Phys. Crystallogr., 19,* 171–174).

Liebau, F. (1972) Silicon crystal chemistry. In K. H. Wedepohl, Ed., *Handbook of Geochemistry,* Vol. II-2. Springer-Verlag, Berlin.

McCauley, J. W. and R. E. Newnham (1971) Origin and prediction of ditrigonal distortions in micas. *Am. Mineral., 56,* 1626–1638.

Morimoto, N. and K. Koto (1969) The crystal structure of orthoenstatite. *Z. Kristallogr., 129,* 65–83.

——, Y. Nakajima, Y. Syono, S. Akimoto and Y. Matsui (1975) Crystal structures of pyroxene-type $ZnSiO_3$ and $ZnMgSi_2O_6$. *Acta Crystallogr., B31,* 1041–1049.

——, C. T. Prewitt, S. Sueno and M. Cameron (1973) Pyroxenes: comparisons of real and ideal structural topologies. *Z. Kristallogr., 138,* 254–273.

—— and M. Ross (1970) Gedrites: crystal structures and intracrystalline cation distributions. *Am. Mineral., 55,* 1945–1972.

Pauling, L. (1948) *The Nature of the Chemical Bond.* Cornell University Press, Ithaca, New York.

Rayner, J. H. and G. Brown (1973) The crystal structure of talc. *Clays and Clay Minerals, 21,* 103–114.

Smith, J. V. (1969) Crystal structure and stability of the $MgSiO_3$ polymorphs: physical properties and phase relations of Mg,Fe pyroxenes. *Mineral. Soc. Am. Spec. Pap., 2,* 3–29.

Smyth, J. R. (1971) Protoenstatite: a crystal-structure refinement at 1100°C. *Z. Kristallogr., 134,* 262–274.

—— (1973) An orthopyroxene structure up to 850°C. *Am. Mineral., 58,* 636–648.

—— (1974) Low orthopyroxene from a lunar deep crustal rock: a new pyroxene polymorph of space group $P2_1ca$. *Geophys. Res. Lett., 1,* 27–29.

—— and C. W. Burnham (1972) The crystal structures of high and low clinohypersthene. *Earth Planet. Sci. Lett., 14,* 183–189.

—— and J. Ito (1977) The synthesis and crystal structure of a magnesium-lithium-scandium protopyroxene. *Am. Mineral., 62,* 1252–1257.

Sueno, S., M. Cameron, J. J. Papike and C. T. Prewitt (1973) The high temperature crystal chemistry of tremolite. *Am. Mineral., 58,* 649–664.

——, —— and C. T. Prewitt (1976) Orthoferrosilite: high-temperature crystal chemistry. *Am. Mineral., 61,* 38–53.

Takeda, H. (1972) Crystallographic studies of coexisting aluminan orthopyroxene and augite of high-pressure origin. *J. Geophys. Res., 77,* 5798–5811.

Thompson, J. B., Jr. (1970) Geometrical possibilities for amphibole structures: model biopyriboles. *Am. Mineral., 55,* 292–293.

—— (1978) Biopyriboles and polysomatic series. *Am. Mineral., 63,* 239–249.

Veblen, D. R. (1976) *Triple- and Mixed-Chain Biopyriboles from Chester, Vermont.* Ph.D. Thesis, Harvard University, Cambridge, Massachusetts.

—— and C. W. Burnham (1975) Triple-chain biopyriboles: newly discovered intermediate products of the retrograde anthophyllite-talc transformation, Chester, Vt. (abstr.). *Trans. Am. Geophys. Union, 56,* 1076.

—— and —— (1976) Biopyriboles from Chester, Vermont: the first mixed-chain silicates (abstr.). *Geol. Soc. Am. Abstracts with Programs, 8,* 1153.

—— and —— (1978) New biopyriboles from Chester, Vermont: I. Descriptive mineralogy. *Am. Mineral., 63,* 1000–1009.

——, P. R. Buseck and C. W. Burnham (1977) Asbestiform chain silicates: new minerals and structural groups. *Science, 198,* 359–365.

Warren, B. E. (1929) The structure of tremolite $H_2Ca_2Mg_5(SiO_3)_8$. *Z. Kristallogr., 72,* 42–57.

—— and D. I. Modell (1930) The structure of anthophyllite $H_2Mg_5(SiO_3)_8$. *Z. Kristallogr., 75,* 161–178.

Manuscript received, October 13, 1977; accepted for publication, May 16, 1978.

The following material did not appear in the original publication.

Veblen, D.R. & C.W.Burnham
New biopyriboles from
Chester, Vermont. II.

Table 5a (part 1 of 2)

M-O Distances, Å

M1 Octahedron	
M1-O2A(1)*	2.082
M1-O2A(2)	2.078
M1-O2B(6)	2.082
M1-O2B(7)	2.083
M1-OHA	2.069
M1-OHB	2.069
Mean	2.077

M2 Octahedron	
M2-OHB	2.066
M2-O2A	2.102
M2-OHA	2.069
M2-O4A	2.075
M2-O2B	2.091
M2-O4B	2.083
Mean	2.081

M3 Octahedron	
M3-OHA	2.097
M3-OHB	2.078
M3-O4A	2.070
M3-O7A	2.104
M3-O4A	2.066
M3-O7B	2.120
Mean	2.089

M4 Octahedron	
M4-O4A	2.151
M4-O4B	2.138
M4-O7B	2.080
M4-O7A	2.077
M4-O8A	2.032
M4-O8B	2.048
Mean	2.087

M5 Octahedron	
M5-O7A	2.167
M5-O7B	2.154
M5-O8A	2.042
M5-O6A	2.443
M5-O6B	2.800
M5-O8B	2.002
M5-O5B	2.938
Si3A-M5	2.889
Mean (6)	2.268

Estimated Standard Error M-O = 0.005Å

O-O Distances in Cation Octahedra, Å

M1 Octahedron	
O2A(1)-O2A(2)	3.050
O2A(1)-OHA(3)	3.080
O2A(2)-OHA(3)	3.076
O2B(6)-O2B(7)	3.054
O2B(6)-OHB(5)	3.079
O2B(7)-OHB(5)	3.078
Mean (6)	3.070
O2A(1)-O2B(6)	2.801
O2A(1)-OHB(5)	2.804
O2A(2)-O2B(6)	2.790
O2A(2)-O2B(7)	2.801
OHA(3)-O2B(7)	2.813
OHA(3)-OHB(5)	2.766
Mean (6)	2.795
Mean (12)	2.933

M2 Octahedron	
O2A-OHA	3.071
O2A-O4A	3.102
OHA-O4A	3.065
O2B-OHB	3.068
O2B-O4B	3.108
OHB-O4B	3.078
Mean (6)	3.082
O2A-O2B	2.790
O2A-OHB	2.804
OHA-O2B	2.813
OHA-O4B	2.801
O4A-OHB	2.779
O4A-O4B	2.793
Mean (6)	2.797
Mean (12)	2.939

M3 Octahedron	
O4A-OHA	3.061
O4A-O7A	3.091
OHA-O7A	3.087
O4B-OHB	3.060
O4B-O7B	3.090
OHB-O7B	3.089
Mean (6)	3.080
O4A-OHB	2.779
O4A-O7B	2.851
OHA-OHB	2.766
OHA-O4B	2.801
O7A-O4B	2.819
O7A-O7B	2.926
Mean (6)	2.824
Mean (12)	2.952

M4 Octahedron	
O4A-O7A	3.044
O4A-O8A	2.994
O7A-O8A	3.077
O4B-O7B	3.036
O4B-O8B	3.060
O7B-O8B	3.096
Mean (6)	3.051
O4A-O4B	2.793
O4A-O7B	2.851
O8A-O7B	2.823
O8A-O8B	2.972
O7A-O4B	2.819
O7A-O8B	2.805
Mean (6)	2.844
Mean (12)	2.948

M5 Octahedron	
O7A-O8A	2.958
O7A-O6A	3.751
O8A-O6A	2.517
O7B-O8B	3.014
O7B-O6B	4.249
O8B-O6B	2.549
Mean (6)	3.173
O7A-O8B	2.805
O7A-O7B	2.926
O8A-O7B	2.823
O8A-O6B	4.310
O6A-O6B	3.019
O6A-O8B	3.790
Mean (6)	3.279
Mean (12)	3.226

Estimated Standard Error O-O = 0.006Å

O-M-O Angles, deg.

M1 Octahedron	
OHA(3)-M1-OHB(5)	84.1
OHA(3)-M1-O2A(1)	95.8
OHA(3)-M1-O2A(2)	95.8
OHA(3)-M1-O2B(7)	85.3
OHB(5)-M1-O2A(1)	85.2
OHB(5)-M1-O2B(6)	95.9
OHB(5)-M1-O2B(7)	95.9
O2A(1)-M1-O2A(2)	94.3
O2A(1)-M1-O2B(6)	84.5
O2A(2)-M1-O2B(6)	84.2
O2A(2)-M1-O2B(7)	84.7
O2B(6)-M1-O2B(7)	94.3
Mean	90.0
OHA(3)-M1-O2B(6)	179.6
OHB(5)-M1-O2A(2)	179.4
O2A(1)-M1-O2B(7)	178.5
Mean	179.2

M2 Octahedron	
OHB-M2-O2A	84.6
OHB-M2-O4A	84.3
OHB-M2-O2B	95.1
OHB-M2-O4B	95.8
O2A-M2-OHA	94.8
O2A-M2-O4A	95.9
O2A-M2-O2B	83.4
OHA-M2-O4A	95.4
OHA-M2-O2B	85.1
OHA-M2-O4B	84.9
O4A-M2-O4B	84.4
O2B-M2-O4B	96.3
Mean	90.0
OHB-M2-OHA	179.3
O2A-M2-O4B	179.5
O4A-M2-O2B	179.2
Mean	179.3

M3 Octahedron	
OHA-M3-OHB	83.0
OHA-M3-O4A	94.5
OHA-M3-O7A	94.6
OHA-M3-O4B	84.6
OHB-M3-O4A	84.1
OHB-M3-O4B	95.2
OHB-M3-O7B	94.7
O4A-M3-O7A	95.6
O4A-M3-O7B	85.8
O7A-M3-O4B	85.1
O7A-M3-O7B	87.7
O4B-M3-O7B	95.1
Mean	90.0
OHA-M3-O7B	177.7
OHB-M3-O7A	177.5
O4A-M3-O4B	179.0
Mean	178.1

M4 Octahedron	
O4A-M4-O4B	81.3
O4A-M4-O7B	84.7
O4A-M4-O7A	92.1
O4A-M4-O8A	91.4
O4B-M4-O7B	92.1
O4B-M4-O7A	83.9
O4B-M4-O8B	93.9
O7B-M4-O8A	86.7
O7B-M4-O8B	97.2
O7A-M4-O8A	97.0
O7A-M4-O8B	85.7
O8A-M4-O8B	93.5
Mean	90.0
O4A-M4-O8B	174.9
O4B-M4-O8A	172.6
O7B-M4-O7A	175.2
Mean	174.2

M5 Octahedron	
O7A-M5-O7B	85.2
O7A-M5-O8A	89.2
O7A-M5-O6A	110.6
O7A-M5-O8B	84.5
O7B-M5-O8A	84.5
O7B-M5-O6B	117.5
O7B-M5-O8B	92.9
O8A-M5-O6A	67.6
O8A-M5-O6B	125.1
O6A-M5-O6B	70.0
O6A-M5-O8B	116.6
O6B-M5-O8B	61.5
Mean	92.1
O7A-M5-O6B	138.4
O7B-M5-O6A	147.0
O8A-M5-O8B	173.4
Mean	152.9

Estimated Standard Error O-M-O = 0.2°

Veblen, D.R. & C.W.Burnham
New biopyriboles from
Chester, Vermont. II.

Table 5a (part 2 of 2)

Si-O Distances, Å

Si1A Tetrahedron		Si2A Tetrahedron		Si3A Tetrahedron	
Si1A-O1A(2)	1.628	Si2A-O3A	1.624	Si3A-O7A	1.618
Si1A-O1A(1)	1.616	Si2A-O4A	1.610	Si3A-O6A	1.673
Si1A-O2A	1.623	Si2A-O5A	1.617	Si3A-O5A	1.628
Si1A-O3A	1.619	Si2A-O6A	1.622	Si3A-O8A	1.595
Mean	1.621	Mean	1.618	Mean	1.628
Si1B Tetrahedron		**Si2B Tetrahedron**		**Si3B Tetrahedron**	
Si1B-O1B(1)	1.621	Si2B-O5B	1.625	Si3B-O6B	1.643
Si1B-O1B(2)	1.630	Si2B-O3B	1.632	Si3B-O5B	1.654
Si1B-O2B	1.619	Si2B-O4B	1.612	Si3B-O7B	1.626
Si1B-O3B	1.619	Si2B-O6B	1.627	Si3B-O8B	1.604
Mean	1.622	Mean	1.624	Mean	1.631

Estimated Standard Error Si-O = 0.005Å

O-O Distances in Si-O Tetrahedra

Si1A Tetrahedron		Si2A Tetrahedron		Si3A Tetrahedron	
O2A-O3A	2.642	O4A-O3A	2.674	O7A-O8A	2.740
O2A-O1A(2)	2.653	O4A-O5A	2.656	O7A-O5A	2.647
O2A-O1A(1)	2.655	O4A-O6A	2.644	O7A-O6A	2.689
O3A-O1A(2)	2.654	O3A-O5A	2.624	O8A-O5A	2.657
O3A-O1A(1)	2.635	O3A-O6A	2.633	O8A-O6A	2.517
O1A-O1A	2.649	O5A-O6A	2.623	O5A-O6A	2.683
Mean	2.648	Mean	2.642	Mean	2.656
Si1B Tetrahedron		**Si2B Tetrahedron**		**Si3B Tetrahedron**	
O2B-O3B	2.636	O4B-O3B	2.690	O7B-O8B	2.745
O2B-O1B(1)	2.649	O4B-O5B	2.645	O7B-O5B	2.658
O2B-O1B(2)	2.647	O4B-O6B	2.637	O7B-O6B	2.648
O3B-O1B(1)	2.635	O3B-O5B	2.654	O8B-O5B	2.653
O3B-O1B(2)	2.661	O3B-O6B	2.642	O8B-O6B	2.549
O1B-O1B	2.666	O5B-O6B	2.642	O5B-O6B	2.723
Mean	2.649	Mean	2.652	Mean	2.663

Estimated Standard Error O-O = 0.006Å

O-Si-O Angles, deg.

Si1A Tetrahedron		Si2A Tetrahedron	
O1A-Si1A-O1A	109.4	O3A-Si2A-O4A	111.6
O3A-Si1A-O1A(1)	109.1	O3A-Si2A-O5A	108.1
O3A-Si1A-O1A(2)	109.7	O3A-Si2A-O6A	108.4
O3A-Si1A-O2A	109.2	O4A-Si2A-O5A	110.8
O2A-Si1A-O1A(2)	109.4	O4A-Si2A-O6A	109.8
O2A-Si1A-O1A(1)	110.1	O5A-Si2A-O6A	108.2
Mean	109.5	Mean	109.8
Si3A Tetrahedron		**Si1B Tetrahedron**	
O7A-Si3A-O6A	109.6	O1B-Si1B-O1B	110.2
O7A-Si3A-O5A	109.3	O3B-Si1B-O1B(1)	108.9
O7A-Si3A-O8A	117.0	O3B-Si1B-O1B(2)	110.0
O6A-Si3A-O5A	108.7	O3B-Si1B-O2B	109.0
O6A-Si3A-O8A	100.7	O2B-Si1B-O1B(1)	109.7
O5A-Si3A-O8A	111.0	O2B-Si1B-O1B(2)	109.1
Mean	109.4	Mean	109.5
Si2B Tetrahedron		**Si3B Tetrahedron**	
O3B-Si2B-O4B	112.0	O7B-Si3B-O6B	108.2
O3B-Si2B-O5B	109.2	O7B-Si3B-O5B	108.3
O3B-Si2B-O6B	108.4	O7B-Si3B-O8B	116.4
O4B-Si2B-O5B	109.6	O6B-Si3B-O5B	111.4
O4B-Si2B-O6B	109.0	O6B-Si3B-O8B	103.5
O5B-Si2B-O6B	108.7	O5B-Si3B-O8B	109.0
Mean	109.5	Mean	109.5

Estimated Standard Error O-Si-O = 0.3°

Tetrahedral Chains

A Chain		B Chain	
Si1A-Si1A	3.053Å	Si1B-Si1B	3.048Å
Si1A-Si2A	3.055	Si1B-Si2B	3.039
Si2A-Si3A(1)	3.084	Si2B-Si3B(1)	3.069
Si2A-Si3A(3)	3.055	Si2B-Si3B(3)	3.052
O1A-O1A-O1A	179.6°	O1B-O1B-O1B	166.9°
O5A-O6A-O5A	173.5	O5B-O6B-O5B	161.7

Estimated Standard Errors Si-Si = 0.003Å
O-O-O = 0.4°

---

* Coordinate transformations indicated in parentheses are as follows:

(1)	x, y, z	(5)	1/2+x, y, 3/2-z
(2)	x, 1/2-y, 1/2+z	(6)	1/2+x, 1/2-y, 1-z
(3)	x, y, 1+z	(7)	1/2-x, y, 3/2-z

Atoms without transformations indicated are in xyz, or are participating in an unambiguous distance or angle.

Veblen, D.R. & C.W.Burnham
New biopyriboles from
Chester, Vermont. II

Table 5b (part 1 of 2)

M-O Distances, Å

M1 Octahedron		M2 Octahedron		M3 Octahedron	
2 M1-OH	2.061	2 M2-OH	2.079	2 M3-OH	2.098
2 M1-O2(1)*	2.072	2 M2-O2	2.086	2 M3-O4	2.073
2 M1-O2(2)	2.078	2 M2-O4	2.081	2 M3-O7	2.097
Mean	2.070	Mean	2.082	Mean	2.089

M4 Octahedron		M5 Octahedron	
2 M4-O4	2.128	2 M5-O7	2.162
2 M4-O7	2.081	2 M5-O8	2.032
2 M4-O8	2.049	2 M5-O6	2.659
Mean	2.086	2 M5-O5	3.106
		2 Si3-M5	2.979
		Mean (6)	2.284

Estimated Standard Error M-O = 0.009Å

O-O Distances in Cation Octahedra, Å

M1 Octahedron		M2 Octahedron	
2 O2(1)-O2(4)	3.06	2 OH(6)-O2(1)	3.09
2 O2(1)-OH(1)	3.07	2 OH(6)-O4(1)	3.08
2 O2(4)-OH(1)	3.07	2 O2(1)-O4(1)	3.11
Mean (6)	3.07	Mean (6)	3.09
2 O2(1)-O2(2)	2.77	2 OH(6)-O2(5)	2.80
2 O2(1)-OH(3)	2.80	2 OH(6)-O4(5)	2.79
1 O2(2)-O2(10)	2.78	1 O2(1)-O2(5)	2.78
1 OH(1)-OH(3)	2.77	1 O4(1)-O4(5)	2.77
Mean (6)	2.78	Mean (6)	2.79
Mean (12)	2.92	Mean (12)	2.94

M3 Octahedron		M4 Octahedron	
2 O4(1)-OH(1)	3.07	2 O7(6)-O4(1)	3.04
2 O4(1)-O7(1)	3.10	2 O7(6)-O8(7)	3.09
2 OH(1)-O7(1)	3.08	2 O4(1)-O8(7)	3.01
Mean (6)	3.08	Mean (6)	3.05
2 O4(1)-OH(3)	2.79	2 O7(6)-O4(5)	2.82
2 O4(1)-O7(3)	2.82	2 O7(6)-O8(11)	2.82
1 OH(1)-OH(3)	2.77	1 O4(1)-O4(5)	2.77
1 O7(1)-O7(3)	2.91	1 O8(7)-O8(11)	3.00
Mean (6)	2.82	Mean (6)	2.84
Mean (12)	2.95	Mean (12)	2.94

O-O Distances In Cation Octahedra, Å (Continued)

M5 Octahedron	
2 O8(7)-O7(1)	2.98
2 O8(7)-O6(7)	2.54
2 O7(1)-O6(7)	4.10
Mean (6)	3.21
2 O8(7)-O7(3)	2.82
2 O8(7)-O6(8)	4.12
1 O7(1)-O7(3)	2.91
1 O6(7)-O6(8)	3.03
Mean (6)	3.30
Mean (12)	3.26

Estimated Standard Error O-O = 0.02Å

O-M-O Angles, deg.

M1 Octahedron		M2 Octahedron	
2 OH(1)-M1-O2(1)	96.0	2 OH(3)-M2-O2(1)	84.5
2 OH(1)-M1-O2(3)	85.3	2 OH(3)-M2-O2(5)	95.6
2 OH(1)-M1-O2(4)	95.8	2 OH(3)-M2-O4(1)	84.4
2 O2(1)-M1-O2(2)	83.9	2 OH(3)-M2-O4(5)	95.5
2 O2(1)-M1-O2(4)	94.9	2 O2(1)-M2-O4(1)	96.5
1 OH(1)-M1-OH(3)	84.4	1 O2(1)-M2-O2(5)	83.6
1 O2(2)-M1-O2(4)	84.0	1 O4(1)-M2-O4(5)	83.4
Mean	90.0	Mean	90.0
2 OH(1)-M1-O2(2)	179.8	2 O2(1)-M2-O4(5)	179.9
1 O2(1)-M1-O2(3)	178.3	1 OH(3)-M2-OH(6)	179.9
Mean	179.3	Mean	179.9

M3 Octahedron		M4 Octahedron	
2 OH(1)-M3-O4(1)	94.9	2 O4(1)-M4-O7(3)	84.1
2 OH(1)-M3-O4(2)	84.1	2 O4(1)-M4-O7(6)	92.4
2 OH(1)-M3-O7(1)	94.7	2 O4(1)-M4-O8(1)	92.3
2 O4(1)-M3-O7(1)	95.9	2 O7(3)-M4-O8(1)	86.1
2 O4(1)-M3-O7(3)	85.1	2 O7(3)-M4-O8(5)	97.1
1 OH(1)-M3-OH(3)	82.6	1 O4(1)-M4-O4(5)	81.2
1 O7(1)-M3-O7(3)	88.0	1 O8(1)-M4-O8(5)	94.2
Mean	90.0	Mean	90.0
2 OH(1)-M3-O7(3)	177.3	2 O4(1)-M4-O8(5)	173.5
1 O4(1)-M3-O4(2)	178.7	1 O7(3)-M4-O7(6)	175.4
Mean	177.8	Mean	174.1

Veblen, D.R. & C.W.Burnham
New biopyriboles from
Chester, Vermont. II.

Table 5b (part 2 of 2)

O-M-O Angles, deg. (Continued)

M5 Octahedron	
2 O7(1)-M5-O8(1)	90.7
2 O7(1)-M5-O6(7)	115.9
2 O7(1)-M5-O8(3)	84.4
2 O8(1)-M5-O6(7)	64.0
2 O8(1)-M5-O6(8)	122.4
1 O7(1)-M5-O7(3)	84.7
1 O6(7)-M5-O6(8)	69.5
Mean	92.4
2 O7(1)-M5-O6(8)	141.1
1 O8(1)-M5-O8(3)	173.3
Mean	151.8

Estimated Standard Error O-M-O = 0.5°

Si-O Distances, Å

Si1 Tetrahedron		Si2 Tetrahedron		Si3 Tetrahedron	
Si1-O1(1)	1.628	Si2-O3	1.606	Si3-O6	1.655
Si1-O1(9)	1.627	Si2-O4	1.613	Si3-O7	1.632
Si1-O2	1.634	Si2-O6	1.642	Si3-O5	1.642
Si1-O3	1.616	Si2-O5	1.628	Si3-O8	1.601
Mean	1.626	Mean	1.622	Mean	1.633

Estimated Standard Error Si-O = 0.009Å

O-O Distances in Si-O Tetrahedra, Å

Si1 Tetrahedron		Si2 Tetrahedron		Si3 Tetrahedron	
O3-O1(1)	2.650	O3-O4	2.663	O8-O5	2.652
O3-O1(9)	2.654	O3-O5	2.626	O8-O6	2.540
O3-O2	2.631	O3-O6	2.628	O8-O7	2.742
O2-O1(1)	2.663	O4-O5	2.661	O7-O5	2.671
O2-O1(9)	2.671	O4-O6	2.678	O7-O6	2.682
O1-O1	2.663	O5-O6	2.638	O5-O6	2.694
Mean	2.655	Mean	2.649	Mean	2.664

Estimated Standard Error O-O = 0.012Å

O-Si-O Angles, deg.

Si1 Tetrahedron		Si2 Tetrahedron	
O3-Si1-O1(1)	109.5	O3-Si2-O4	111.6
O3-Si1-O1(9)	109.9	O3-Si2-O5	108.5
O3-Si1-O2	108.1	O3-Si2-O6	108.0
O2-Si1-O1(1)	109.5	O4-Si2-O5	110.4
O2-Si1-O1(9)	110.0	O4-Si2-O6	110.7
O1-Si1-O1	109.8	O5-Si2-O6	107.5
Mean	109.5	Mean	109.5

Si3 Tetrahedron	
O8-Si3-O7	116.0
O8-Si3-O5	109.7
O8-Si3-O6	102.5
O7-Si3-O5	109.3
O7-Si3-O6	109.3
O5-Si3-O6	109.6
Mean	109.4

Estimated Standard Error O-Si-O = 0.5°

Tetrahedral Chain

Si1-Si1	3.055Å
Si1-Si2	3.043
Si2-Si3(1)	3.090
Si2-Si3(6)	3.056
O1-O1-O1	171.4°
O5-O6-O5	170.0

Estimated Standard Errors Si-Si = 0.004Å
O-O-O = 0.6°

* Coordinate transformations indicated in parentheses are as follows:

(1) x, y, z	(7) 1/2-x, 1/2-y, 1-z
(2) -x,-y, 1-z	(8) x-1/2, 1/2-y, z-1/2
(3) -x, y, 1/2-z	(9) x, -y, 1/2+z
(4) x, -y, z-1/2	(10) -x, -y, 1-z
(5) -x, y, 3/2-z	(11) x-1/2, 1/2-y, 1/2+z
(6) x, y, 1+z	

Atoms without transformations indicated are in xyz, or are participating in an unambiguous distance or angle. Numerals preceeding bonds and angles indicate multiplicity.

Table 5c (part 1 of 3)

M-O Distances, Å

MT1 Octahedron		MT2 Octahedron		MT3 Octahedron	
MT1-OT2A(3)*	2.05	MT2-OHTA	2.10	MT3-OHTA	2.10
MT1-OT2A(2)	2.07	MT2-OHTB	2.06	MT3-OHTB	2.07
MT1-OT2B(4)	2.11	MT2-OT2A	2.11	MT3-OT4A	2.05
MT1-OT2B(5)	2.12	MT2-OT2B	2.10	MT3-OT4B	2.08
MT1-OHTA	2.02	MT2-OT4A	2.09	MT3-OT7A	2.06
MT1-OHTB	2.07	MT2-OT4B	2.04	MT3-OT7B	2.16
Mean	2.07	Mean	2.08	Mean	2.09
MT4 Octahedron		**MT5 Octahedron**		**MD3 Octahedron**	
MT4-OT4A	2.16	MT5-OT7A	2.15	2 MD3-OD1A	2.10
MT4-OT4B	2.16	MT5-OT7B	2.20	2 MD3-OD1B	2.10
MT4-OT7A	2.07	MT5-OD4A	2.04	MD3-OHDA	2.04
MT4-OT7B	2.10	MT5-OD4B	1.99	MD3-OHDB	2.09
MT4-OD4A	2.00	MT5-OD6A	2.42	Mean	2.09
MT4-OD4B	2.02	MT5-OD6B	2.82		
Mean	2.09	MT5-OD5B	2.92		
		SiD2A-MT5	2.91		
		Mean (6)	2.27		
MD1 Octahedron		**MD2 Octahedron**		**MD4 Octahedron**	
MD1-OD1A	2.11	MD2-OD1A	2.12	MD4-OD2A	2.19
MD1-OD1B	2.03	MD2-OD1B	2.11	MD4-OD2B	2.13
MD1-OD2A	2.16	MD2-OD2A	2.10	MD4-OT8A	2.02
MD1-OD2B	2.11	MD2-OD2B	2.06	MD4-OT8B	2.02
MD1-OHDA	2.11	MD2-OT8A	2.07	MD4-OT6A	2.44
MD1-OHDB	2.08	MD2-OT8B	2.06	MD4-OT6B	2.81
Mean	2.10	Mean	2.09	MD4-OD5B	2.96
				SiT3A-MD4	2.87
				Mean (6)	2.27

Estimated Standard Error M-O = 0.02Å

O-O Distances in Cation Octahedra, Å

MT1 Octahedron		MT2 Octahedron		MT3 Octahedron	
OHTA(1)-OT2A(2)	3.07	OHTA-OT4A	3.09	OT4A-OHTA	3.06
OHTA(1)-OT2A(3)	3.03	OHTA-OT2A	3.06	OT4A-OT7A	3.08
OT2A(2)-OT2A(3)	3.07	OH4A-OT2A	3.07	OHTA-OT7A	3.12
OHTB(6)-OT2B(4)	3.08	OHTB-OT4B	3.08	OT4B-OHTB	3.03
OHTB(6)-OT2B(5)	3.09	OHTB-OT2B	3.10	OT4B-OT7B	3.11
OT2B(5)-OT2B(6)	3.04	OT4B-OT2B	3.11	OHTB-OT7B	3.05
Mean (6)	3.06	Mean (6)	3.09	Mean (6)	3.08
OT2A(3)-OHTB(6)	2.76	OHTA-OT4B	2.82	OT4A-OHTB	2.73
OT2A(3)-OT2B(4)	2.82	OHTA-OT2B	2.85	OT4A-OT7B	2.85
OT2B(5)-OHTA(1)	2.85	OHTB-OT4A	2.73	OT4B-OHTA	2.82
OT2B(5)-OT2A(2)	2.82	OHTB-OT2A	2.76	OT4B-OT7A	2.82
OT2A(2)-OT2B(4)	2.80	OT4A-OT4B	2.78	OHTA-OHTB	2.74
OHTA(1)-OHTB(6)	2.74	OT2A-OT2B	2.80	OT7A-OT7B	2.94
Mean (6)	2.80	Mean (6)	2.79	Mean (6)	2.82
Mean (12)	2.93	Mean (12)	2.94	Mean (12)	2.95

O-O Distances in Cation Octahedra, Å (Continued)

MT4 Octahedron		MT5 Octahedron			MD3 Octahedron	
OT7A-OT4A	3.07	OD4A-OD6A	2.53	2	OHDA-OD1A	3.09
OT7A-OD4A	3.07	OD4A-OT7A	2.93	1	OD1A-OD1A	3.20
OT4A-OD4A	2.96	OD6A-OT7A	3.76	2	OHDB-OD1B	3.07
OT7B-OT4B	3.02	OD4B-OD6B	2.53	1	OD1B-OD1B	3.14
OT7B-OD4B	3.10	OD4B-OT7B	3.07		Mean (6)	3.11
OT4B-OD4B	3.11	OD6B-OT7B	4.30	2	OHDA-OD1B	2.74
Mean (6)	3.06	Mean (6)	3.19	2	OHDB-OD1A	2.86
OT7A-OT4B	2.82	OD4A-OD6B	4.35	2	OD1A-OD1B	2.75
OT7A-OD4B	2.76	OD4A-OT7B	2.84		Mean (6)	2.78
OT7B-OT4A	2.85	OD4B-OD6A	3.72		Mean (12)	2.95
OT7B-OD4A	2.84	OD4B-OT7A	2.76			
OT4A-OT4B	2.78	OT7A-OT7B	2.94			
OD4A-OD4B	2.92	OD6A-OD6B	3.03			
Mean (6)	2.83	Mean (6)	3.27			
Mean (12)	2.94	Mean (12)	3.23			
MD1 Octahedron		**MD2 Octahedron**			**MD4 Octahedron**	
OD1A-OHDA	3.10	OD2A-OD1A	3.00		OT8A-OD2A	3.00
OD1A-OD2A	3.09	OD2A-OT8A	3.10		OT8A-OT6A	2.48
OHDA-OD2A	3.10	OD1A-OT8A	3.02		OD2A-OT6A	3.83
OD1B-OHDB	3.09	OD2B-OD1B	3.05		OT8B-OD2B	3.00
OD1B-OD2B	3.11	OD2B-OT8B	3.08		OT8B-OT6B	2.56
OHDB-OD2B	3.13	OD1B-OT8B	3.05		OD2B-OT6B	4.24
Mean (6)	3.10	Mean (6)	3.05		Mean (6)	3.19
OD1A-OHDB	2.86	OD2A-OD1B	2.80		OT8A-OT6B	4.27
OD1A-OD2B	2.85	OD2A-OT8B	2.85		OT8A-OD2B	2.82
OD1B-OHDA	2.74	OD2B-OD1A	2.85		OT8B-OT6A	3.81
OD1B-OD2A	2.80	OD2B-OT8A	2.82		OT8B-OD2A	2.85
OHDA-OHDB	2.78	OD1A-OD1B	2.75		OD2A-OD2B	2.95
OD2A-OD2B	2.95	OT8A-OT8B	2.98		OT6A-OT6B	3.00
Mean (6)	2.83	Mean (6)	2.84		Mean (6)	3.28
Mean (12)	2.97	Mean (12)	2.95		Mean (12)	3.23

Estimated Standard Error O-O = 0.03Å

O-M-O Angles, deg.

MT1 Octahedron		MT2 Octahedron	
OHTA(1)-MT1-OHTB(6)	84.1	OHTA-MT2-OT2B	85.6
OHTA(1)-MT1-OT2A(3)	96.2	OHTA-MT2-OT2A	93.3
OHTA(1)-MT1-OT2A(2)	96.9	OHTA-MT2-OT4A	95.2
OHTA(1)-MT1-OT2B(5)	87.0	OHTA-MT2-OT4B	86.0
OHTB(6)-MT1-OT2A(3)	84.3	OT2B-MT2-OHTB	96.5
OHTB(6)-MT1-OT2B(4)	94.9	OT2B-MT2-OT2A	83.7
OHTB(6)-MT1-OT2B(5)	95.1	OT2B-MT2-OT4B	97.4
OT2A(3)-MT1-OT2A(2)	96.3	OHTB-MT2-OT2A	83.2
OT2A(3)-MT1-OT2B(4)	85.1	OHTB-MT2-OT4A	82.5
OT2A(2)-MT1-OT2B(4)	84.1	OHTB-MT2-OT4B	97.4
OT2A(2)-MT1-OT2B(5)	84.4	OT2A-MT2-OT4A	94.1
OT2B(4)-MT1-OT2B(5)	91.7	OT4A-MT2-OT4B	84.8
Mean	90.0	Mean	90.0
OHTA(1)-MT1-OT2B(4)	178.3	OHTA-MT2-OHTB	175.7
OHTB(6)-MT1-OT2A(2)	178.8	OT2B-MT2-OT4A	177.7
OT2A(2)-MT1-OT2B(5)	176.7	OT2A-MT2-OT4B	178.6
Mean	177.9	Mean	177.3

Table 5c (part 2 of 3)

O-M-O Angles, deg. (Continued)

MT3 Octahedron	
OHTA-MT3-OHTB	82.0
OHTA-MT3-OT4B	84.9
OHTA-MT3-OT4A	95.1
OHTA-MT3-OT7A	97.2
OHTB-MT3-OT4B	93.8
OHTB-MT3-OT4A	83.3
OHTB-MT3-OT7B	92.5
OT4B-MT3-OT7A	85.8
OT4B-MT3-OT7B	94.3
OT4A-MT3-OT7A	97.1
OT4A-MT3-OT7B	85.5
OT7A-MT3-OT7B	88.3
Mean	90.0
OHTA-MT3-OT7B	174.4
OHTB-MT3-OT7A	179.2
OT4B-MT3-OT4A	177.1
Mean	176.9
MT5 Octahedron	
OT7A-MT5-OT7B	85.1
OT7A-MT5-OD4B	83.7
OT7A-MT5-OD6A	110.9
OT7A-MT5-OD4A	88.9
OT7B-MT5-OD4B	94.0
OT7B-MT5-OD4A	84.2
OT7B-MT5-OD6B	117.1
OD4B-MT5-OD6A	115.1
OD4B-MT5-OD6B	60.7
OD6A-MT5-OD4A	68.7
OD6A-MT5-OD6B	70.2
OD4A-MT5-OD6B	126.6
Mean	92.1
OT7A-MT5-OD6B	137.8
OT7B-MT5-OD6A	147.5
OD4B-MT5-OD4A	172.5
Mean	152.6
MD2 Octahedron	
OT8A-MD2-OT8B	92.3
OT8A-MD2-OD1A	92.2
OT8A-MD2-OD2A	96.2
OT8A-MD2-OD2B	86.1
OT8B-MD2-OD2A	86.4
OT8B-MD2-OD2B	96.9
OT8B-MD2-OD1B	94.3
OD1A-MD2-OD2A	90.6
OD1A-MD2-OD2B	86.0
OD1A-MD2-OD1B	81.2
OD2A-MD2-OD1B	83.4
OD2B-MD2-OD1B	93.9
Mean	90.0
OT8A-MD2-OD1B	173.4
OT8B-MD2-OD1A	174.8
OD2A-MD2-OD2B	175.9
Mean	174.7

MT4 Octahedron	
OT4A-MT4-OT4B	80.1
OT4A-MT4-OT7A	93.0
OT4A-MT4-OT7B	84.1
OT4A-MT4-OD4A	90.8
OT4B-MT4-OT7A	83.5
OT4B-MT4-OT7B	90.3
OT4B-MT4-OD4B	96.0
OT7A-MT4-OD4A	98.0
OT7A-MT4-OD4B	85.0
OT7B-MT4-OD4A	87.8
OT7B-MT4-OD4B	97.6
OD4A-MT4-OD4B	93.1
Mean	89.9
OT4A-MT4-OD4B	175.9
OT4B-MT4-OD4A	170.9
OT7A-MT4-OT7B	173.6
Mean	173.5
MD1 Octahedron	
OD1A-MD1-OD2A	92.6
OD1A-MD1-OD2B	85.0
OD1A-MD1-OHDB	86.1
OD1A-MD1-OHDA	94.7
OD2A-MD1-OD2B	87.2
OD2A-MD1-OD1B	83.7
OD2A-MD1-OHDA	93.2
OD2B-MD1-OD1B	97.3
OD2B-MD1-OHDB	96.6
OD1B-MD1-OHDB	97.5
OD1B-MD1-OHDA	83.1
OHDB-MD1-OHDA	83.0
Mean	90.0
OD1A-MD1-OD1B	175.6
OD2A-MD1-OHDB	175.9
OD2B-MD1-OHDA	179.5
Mean	177.0
MD4 Octahedron	
OT6A-MD4-OT8A	66.6
OT6A-MD4-OT6B	69.1
OT6A-MD4-OD2A	111.1
OT6A-MD4-OT8B	116.9
OT8A-MD4-OT6B	123.3
OT8A-MD4-OD2A	90.6
OT8A-MD4-OD2B	85.4
OT6B-MD4-OD2B	117.3
OT6B-MD4-OT8B	61.6
OD2A-MD4-OD2B	85.8
OD2A-MD4-OT8B	85.0
OD2B-MD4-OT8B	92.3
Mean	92.1
OT6B-MD4-OD2A	138.5
OT6A-MD4-OD2B	146.6
OT8A-MD4-OT8B	175.2
Mean	153.4

O-M-O Angles, deg. (Continued)

MD3 Octahedron	
2 OD1A(1)-MD3-OD1B(7)	81.8
2 OD1A-MD3-OHDA	96.6
2 OD1A-MD3-OHDB	86.3
2 OHDA-MD3-OD1B	82.9
2 OHDB-MD3-OD1B	94.2
1 OD1A-MD3-OD1A	99.5
1 OD1B-MD3-OD1B	96.9
Mean	90.0
2 OD1A(1)-MD3-OD1B(8)	178.7
1 OHDA-MD3-OHDB	175.6
Mean	177.7

Estimated Standard Error O-M-O = 0.6°

Si-O Distances, Å

SiT1A Tetrahedron		**SiT2A Tetrahedron**		**SiT3A Tetrahedron**	
SiT1A-OT1A(1)	1.608	SiT2A-OT3A	1.639	SiT3A-OT5A	1.623
SiT1A-OT1A(9)	1.627	SiT2A-OT4A	1.629	SiT3A-OT7A	1.669
SiT1A-OT2A	1.640	SiT2A-OT5A	1.618	SiT3A-OT6A	1.667
SiT1A-OT3A	1.597	SiT2A-OT6A	1.609	SiT3A-OT8A	1.551
Mean	1.618	Mean	1.624	Mean	1.628
SiT1B Tetrahedron		**SiT2B Tetrahedron**		**SiT3B Tetrahedron**	
SiT1B-OT1B(1)	1.660	SiT2B-OT5B	1.648	SiT3B-OT5B	1.630
SiT1B-OT1B(9)	1.601	SiT2B-OT3B	1.632	SiT3B-OT7B	1.572
SiT1B-OT2B	1.554	SiT2B-OT4B	1.585	SiT3B-OT6B	1.667
SiT1B-OT3B	1.615	SiT2B-OT6B	1.635	SiT3B-OT8B	1.600
Mean	1.608	Mean	1.625	Mean	1.617
SiD1A Tetrahedron		**SiD2A Tetrahedron**			
SiD1A-OD6A	1.646	SiD2A-OD4A	1.647		
SiD1A-OD1A	1.589	SiD2A-OD2A	1.559		
SiD1A-OD7A	1.616	SiD2A-OD5A	1.622		
SiD1A-OD5A	1.599	SiD2A-OD6A	1.680		
Mean	1.613	Mean	1.627		
SiD1B Tetrahedron		**SiD2B Tetrahedron**			
SiD1B-OD1B	1.689	SiD2B-OD2B	1.655		
SiD1B-OD5B	1.604	SiD2B-OD4B	1.618		
SiD1B-OD6B	1.636	SiD2B-OD6B	1.603		
SiD1B-OD7B	1.607	SiD2B-OD5B	1.655		
Mean	1.634	Mean	1.633		

Estimated Standard Error Si-O = 0.018Å

O-O Distances in Tetrahedra, Å

SiT1A Tetrahedron		**SiT2A Tetrahedron**		**SiT3A Tetrahedron**	
OT3A-OT1A(1)	2.61	OT3A-OT5A	2.65	OT8A-OT5A	2.62
OT3A-OT1A(9)	2.66	OT3A-OT6A	2.62	OT8A-OT6A	2.48
OT3A-OT2A	2.62	OT3A-OT4A	2.67	OT8A-OT7A	2.75
OT2A-OT1A(1)	2.66	OT4A-OT5A	2.67	OT7A-OT5A	2.66
OT2A-OT1A(9)	2.66	OT4A-OT6A	2.67	OT7A-OT6A	2.74
OT1A-OT1A	2.65	OT5A-OT6A	2.62	OT5A-OT6A	2.68
Mean	2.64	Mean	2.65	Mean	2.66

Table 5c (part 3 of 3)

O-O Distances in Tetrahedra, Å (Continued)

SiT1B Tetrahedron		SiT2B Tetrahedron		SiT3B Tetrahedron	
OT3B-OT1B(1)	2.65	OT3B-OT5B	2.67	OT8B-OT5B	2.65
OT3B-OT1B(9)	2.63	OT3B-OT6B	2.63	OT8B-OT6B	2.56
OT3B-OT2B	2.63	OT3B-OT4B	2.69	OT8B-OT7B	2.71
OT2B-OT1B(1)	2.61	OT4B-OT5B	2.64	OT7B-OT5B	2.57
OT2B-OT1B(9)	2.57	OT4B-OT6B	2.64	OT7B-OT6B	2.62
OT1B-OT1B	2.66	OT5B-OT6B	2.65	OT5B-OT6B	2.72
Mean	2.63	Mean	2.65	Mean	2.64
SiD1A Tetrahedron		SiD2A Tetrahedron			
OD7A-OD5A	2.60	OD4A-OD5A	2.71		
OD7A-OD6A	2.66	OD4A-OD6A	2.53		
OD7A-OD1A	2.65	OD4A-OD2A	2.74		
OD1A-OD5A	2.62	OD2A-OD5A	2.61		
OD1A-OD6A	2.63	OD2A-OD6A	2.64		
OD5A-OD6A	2.64	OD5A-OD6A	2.67		
Mean	2.63	Mean	2.65		
SiD1B Tetrahedron		SiD2B Tetrahedron			
OD7B-OD5B	2.63	OD4B-OD5B	2.63		
OD7B-OD6B	2.66	OD4B-OD6B	2.53		
OD7B-OD1B	2.66	OD4B-OD2B	2.78		
OD1B-OD5B	2.70	OD2B-OD5B	2.68		
OD1B-OD6B	2.69	OD2B-OD6B	2.66		
OD5B-OD6B	2.67	OD5B-OD6B	2.70		
Mean	2.67	Mean	2.66		

Estimated Standard Error O-O = 0.03Å

O-Si-O Angles, deg.

SiT1A Tetrahedron		SiT2A Tetrahedron	
OT3A-SiT1A-OT1A(1)	108.8	OT3A-SiT2A-OT5A	108.7
OT3A-SiT1A-OT1A(9)	111.2	OT3A-SiT2A-OT6A	107.7
OT3A-SiT1A-OT2A	107.8	OT3A-SiT2A-OT4A	109.8
OT2A-SiT1A-OT1A(1)	110.0	OT4A-SiT2A-OT5A	110.6
OT2A-SiT1A-OT1A(9)	109.1	OT4A-SiT2A-OT6A	111.3
OT1A-SiT1A-OT1A	109.9	OT5A-SiT2A-OT6A	108.7
Mean	109.5	Mean	109.5
SiT3A Tetrahedron		SiT1B Tetrahedron	
OT8A-SiT3A-OT5A	111.4	OT3B-SiT1B-OT1B(1)	108.3
OT8A-SiT3A-OT6A	100.6	OT3B-SiT1B-OT1B(9)	109.9
OT8A-SiT3A-OT7A	117.0	OT3B-SiT1B-OT2B	111.9
OT7A-SiT3A-OT5A	107.8	OT2B-SiT1B-OT1B(1)	108.3
OT7A-SiT3A-OT6A	110.4	OT2B-SiT1B-OT1B(9)	108.9
OT5A-SiT3A-OT6A	109.2	OT1B-SiT1B-OT1B	109.6
Mean	109.4	Mean	109.5
SiT2B Tetrahedron		SiT3B Tetrahedron	
OT3B-SiT2B-OT5B	109.1	OT8B-SiT3B-OT5B	110.3
OT3B-SiT2B-OT6B	107.1	OT8B-SiT3B-OT6B	103.4
OT3B-SiT2B-OT4B	113.3	OT8B-SiT3B-OT7B	117.2
OT4B-SiT2B-OT5B	109.4	OT7B-SiT3B-OT5B	106.9
OT4B-SiT2B-OT6B	110.1	OT7B-SiT3B-OT6B	107.9
OT5B-SiT2B-OT6B	107.7	OT5B-SiT3B-OT6B	111.1
Mean	109.5	Mean	109.5

O-Si-O Angles, deg. (Continued)

SiD1A Tetrahedron		SiD2A Tetrahedron	
OD7A-SiD1A-OD5A	107.8	OD4A-SiD2A-OD5A	112.1
OD7A-SiD1A-OD6A	109.3	OD4A-SiD2A-OD6A	99.0
OD7A-SiD1A-OD1A	111.7	OD4A-SiD2A-OD2A	117.5
OD1A-SiD1A-OD5A	110.5	OD2A-SiD2A-OD5A	110.1
OD1A-SiD1A-OD6A	108.6	OD2A-SiD2A-OD6A	109.1
OD5A-SiD1A-OD6A	108.8	OD5A-SiD2A-OD6A	108.2
Mean	109.5	Mean	109.3
SiD1B Tetrahedron		SiD2B Tetrahedron	
OD7B-SiD1B-OD5B	109.9	OD4B-SiD2B-OD5B	107.2
OD7B-SiD1B-OD6B	110.0	OD4B-SiD2B-OD6B	103.7
OD7B-SiD1B-OD1B	107.9	OD4B-SiD2B-OD2B	116.4
OD1B-SiD1B-OD5B	110.1	OD2B-SiD2B-OD5B	108.2
OD1B-SiD1B-OD6B	108.2	OD2B-SiD2B-OD6B	109.3
OD5B-SiD1B-OD6B	110.8	OD5B-SiD2B-OD6B	112.0
Mean	109.5	Mean	109.5

Estimated Standard Error O-Si-O = 0.9°

Tetrahedral Chains

A Triple Chain		B Triple Chain	
SiT1A-SiT1A	3.055Å	SiT1B-SiT1B	3.066Å
SiT1A-SiT2A	3.063	SiT1B-SiT2B	3.008
SiT2A-SiT3A(1)	3.060	SiT2B-SiT3B(1)	3.059
SiT2A-SiT3A(10)	3.060	SiT2B-SiT3B(10)	3.090
OT1A-OT1A-OT1A	179.6°	OT1B-OT1B-OT1B	167.3°
OT5A-OT6A-OT5A	173.5	OT5B-OT6B-OT5B	161.1
A Double Chain		B Double Chain	
SiD1A-SiD1A	3.050Å	SiD1B-SiD1B	3.045Å
SiD1A-SiD2A(1)	3.030	SiD1B-SiD2B(1)	3.042
SiD1A-SiD2A(3)	3.101	SiD1B-SiD2B(10)	3.034
OD5A-OD6A-OD5A	170.6°	O5B-O6B-O5B	161.2°

Estimated Standard Errors Si-Si = 0.013Å
O-O-O = 1.3°

* Coordinate transformations indicated in parentheses are as follows:

(1) x, y, z	(6) x-1/2, y, -z
(2) x, 1/2-y, z-1/2	(7) x, y, z-1
(3) x, y, z-1	(8) x, 1-y, z-1
(4) x-1/2,1/2-y, 1/2-z	(9) x, 1/2-y, 1/2+z
(5) x-1/2,y, 1-z	(10) x, y, 1+z

Atoms without transformations indicated are in xyz, or are participating in an unambiguous distance or angle. Numerals preceeding bonds and angles indicate multiplicity.

Si-O-Si Angles, deg.

Jimthompsonite

Si1A-O1A-Si1A	140.4(3)	Si1B-O1B-Si1B	139.3(3)
Si1A-O3A-Si2A	140.8(3)	Si1B-O3B-Si2B	138.5(3)
Si2A-O5A-Si3A	140.6(3)	Si2B-O5B-Si3B	137.1(3)
Si2A-O6A-Si3A	138.8(3)	Si2B-O6B-Si3B	139.7(3)
Mean	140.2	Mean	138.7

Clinojimthompsonite

Si1-O1-Si1	139.7(7)
Si1-O3-Si2	141.6(5)
Si2-O5-Si3	138.4(6)
Si2-O6-Si3	139.2(6)
Mean	139.7

Chesterite

	SiT1A-OT1A-SiT1A	141.6(1.)	SiT1B-OT1B-SiT1B	140.1(1.1)
	SiT1A-OT3A-SiT2A	142.4(1.)	SiT1B-OT3B-SiT2B	135.8(1.)
	SiT2A-OT5A-SiT3A	141.5(1.)	SiT2B-OT5B-SiT3B	137.9(9)
	SiT2A-OT6A-SiT3A	138.2(1.)	SiT2B-OT6B-SiT3B	138.7(1.)
	Mean	140.9	Mean	138.1
1	SiD1A-OD7A-SiD1A	141.3(1.5)	1 SiD1B-OD7B-SiD1B	142.7(1.5)
2	SiD1A-OD5A-SiD2A	140.4(1.1)	2 SiD1B-OD5B-SiD2B	137.1(1.)
2	SiD1A-OD6A-SiD2A	137.6(1.)	2 SiD1B-OD6B-SiD2B	139.9(1.1)
	Mean	139.5	Mean	139.3

Veblen + Burnham II. Last page of Table 5. (To be deposited).

End of supplemental material.